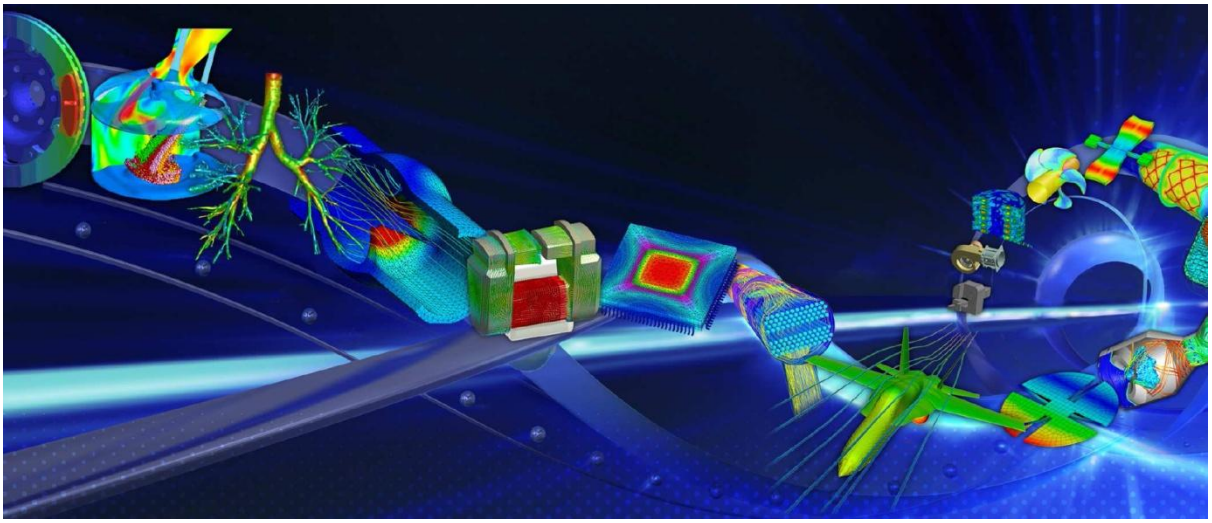

AUTODYN® Composite Modelling
Revision 1.3

ANSYS, Inc.
Southpointe
275 Technology Drive
Canonsburg, PA 15317
ansysinfo@ansys.com
http://www.ansys.com
(T) 724-746-3304
(F) 724-514-9494

Release 14.0
November 2011

ANSYS, Inc. is certified to ISO 9001:2008.

Preface

The AUTODYN hydrocode has extensive capabilities for the modelling of composite materials subjected to a range of loading conditions. A simple linear-elastic orthotropic constitutive model, inherent in which is a linear equation of state, suitable for modelling applications subjected to structural (rather than shock) type loading can be used. Or, for applications such as hypervelocity impacts where the shock effects are obviously important, the orthotropic model can be coupled with non-linear equations of state. Non-linear stress-strain behaviour can also be included through a generalised quadratic plasticity surface and damage can be treated either as brittle damage or softening behaviour can be modelled through an orthotropic damage model.

This document provides a single point of reference for using these models and details all of the above options. Often the greatest difficulty in using such models is a lack of available material data or not knowing how to properly characterise the material should experimental facilities be available. Therefore this document also provides a description of material characterisation experiments that may be performed in order to calculate the required material input parameters.

Table of Contents

1 Introduction

ANSYS AUTODYN is an integrated analysis program designed for non-linear dynamics problems. There is at times a need to consider the treatment of materials where the properties of materials are not identical in all directions (composite laminates, fibre reinforced materials etc.). Material models suitable for such anisotropic material behaviour have been developed in AUTODYN. These models have differing levels of complexity and require differing amounts of material data as input.

The purpose of this document is to fully describe the composite material modelling capabilities of AUTODYN. Further guidance is offered to help the user select the most appropriate models for a specific application and to obtain the relevant material data.

After describing, in 2, the definition of the principal directions in AUTODYN, the material models are presented for both the constitutive behaviour and for predicting failure/damage in 3 and 4 respectively. The most common problems in using such models are the lack of material data and the difficulty in obtaining the measurements. In 5 a series of experimental tests are presented which have been used in projects at ANSYS to successfully characterise various composite materials. Derivation of the model parameters from the experiments is not always straightforward. 6 outlines the required steps in extracting the parameters from experiment into a form suitable for input into AUTODYN.

Example applications are presented in 7 and recommendations on how to perform a typical composite analysis are discussed in 8.

2 Principal Directions in AUTODYN

An orthotropic material has properties that are different in three mutually perpendicular directions and has three mutually perpendicular planes of material symmetry. Thus the properties of such a material are a function of orientation of the material with respect to the global co-ordinate system. The orthotropic constitutive models to be described in 3 are done so in terms of the principal material directions. It is therefore required to define the initial orientation of these principal material directions in an AUTODYN model with respect to the global co-ordinates. Definition of the principal material direction is now described in Section 2.1 for AUTODYN-2D and in Section 2.2 for AUTODYN-3D.

2.1 AUTODYN-2D

For Lagrange and ALE subgrids, two of the principal directions lie in the XY plane. For planar symmetry the third principal direction is perpendicular to the XY plane, and for axial symmetry in AUTODYN-2D the third principal direction is the hoop direction (this direction is termed as either TT or 33 in AUTODYN-2D).

The first principal direction is defined as the angle, in degrees, between the principal direction and the global XY axes. This angle, which can be examined or plotted as a time-history, is called "P.ST.ANG". The second principal direction is orthogonal to the first principal direction in the XY plane. You can plot the principal directions using the "Direction" menu option.

You are allowed to define the initial orientation of the principal material axes in one of three ways. In all three cases, a rotation angle, β, can be specified. If this angle is non-zero, the first and second principal axes are additionally rotated anti-clockwise through this angle.

2.1.1 X-Y Space

The first principal axis is defined relative to X-axis.

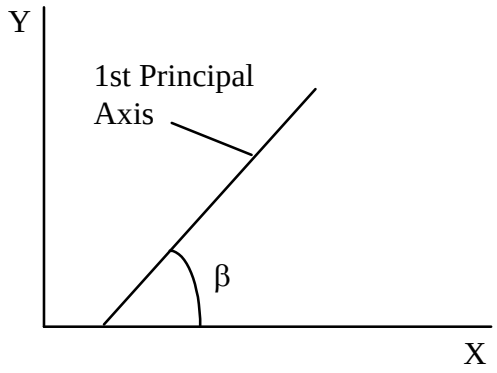

Figure 2-1 Material directions in X-Y space

2.1.2 Polar Space

The first principal axis for each cell is relative to the direction of the line drawn from the polar origin to the centre of the cell.

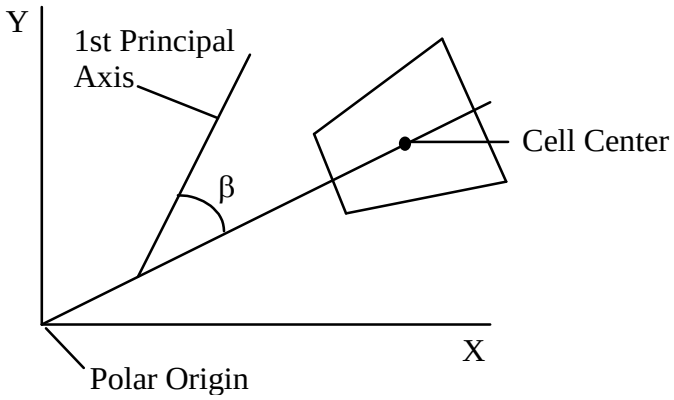

Figure 2-2 Material directions in polar space

2.1.3 I-J Space

The first principal axis for each cell is relative to the direction of increasing I for that cell.

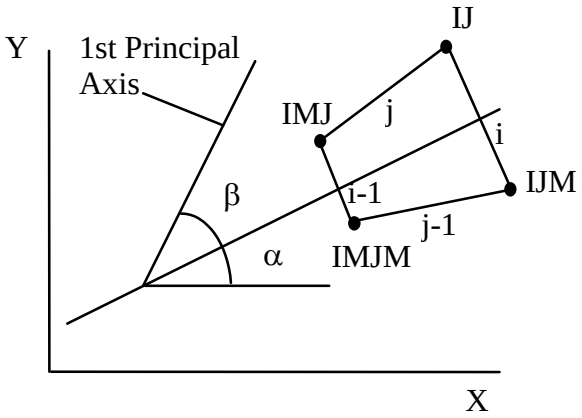

Figure 2-3 Material directions in I-J space

where,

$$\tan\alpha = \frac{Y_{ij} + Y_{ijm} - Y_{imj} - Y_{imjm}}{X_{ij} + X_{ijm} - X_{imj} - X_{imjm}} \qquad (2\text{-}1)$$

2.2 AUTODYN-3D

For 3D Lagrange and ALE subgrids, the three principal directions are oriented in XYZ space and are mutually perpendicular. These three directions are defined by the use of four variables as explained below, and illustrated in Figure 2-4.

The first principal direction is a vector in XYZ space (1 in Figure 2-4) and is defined in AUTODYN-3D by the x, y and z components of this vector. The second and third principal directions are two vectors (2 and 3) which lie in a plane that has it's normal as the first principal direction. The location of the second and third principal directions are defined in AUTODYN-3D by a single angle; this angle (α) is defined as being that between the second principal direction and the vector (2') which is the cross-product (i.e. is normal to) the X axis and the first principal direction. In Figure 2-4, as an example, the direction 1 is shown as vector which is rotated in the XY plane by an angle θ; therefore the direction 2' is coincident with direction Z. The

direction 2 is rotated from 2' by an angle α in the 23 plane. Note that the principal angle can vary between -90° and +90°. Direction 3 is normal to directions 1 and 2.

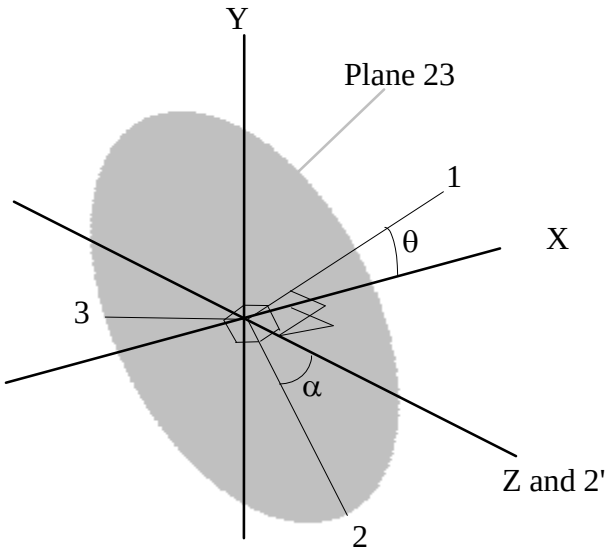

Figure 2-4 Material directions in AUTODYN-3D defined in XYZ-space

You are allowed to define the initial orientation of the principal material axes in one of two ways, as shown below:

2.2.1 X-Y-Z Space

The first principal direction is defined relative to X-Y-Z axes using the x, y and z components of the vector defining the direction. Directions 2 and 3 are defined using the angle α as explained above

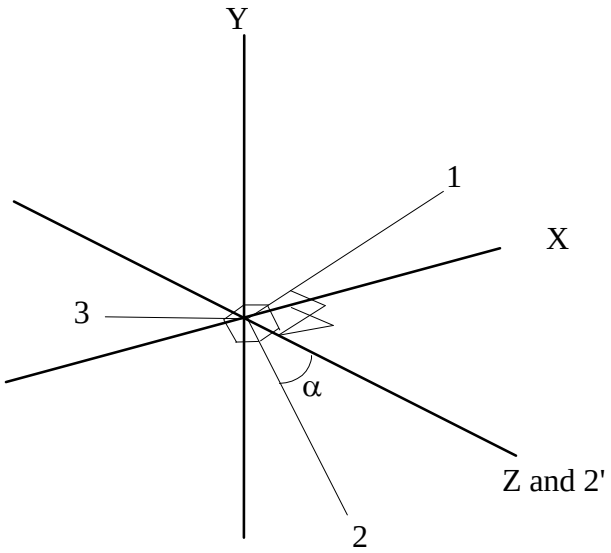

Figure 2-5 Material directions in AUTODYN-3D defined in XYZ-space

2.2.2 I-J-K Space

The first principal direction for each cell is relative to the direction of increasing I for each cell, as shown below. The directions are calculated individually for each cell when the material is filled into the cells; then the directions are stored as four variables exactly as for the X-Y-Z space option. The directions are found as follows:

- The direction 1 is a vector from the centroid of the cell face I-1 (point a) to the centroid of cell face I (point b)
- Next find the midpoints of the K-lines at [I-1,J-1] and [I,J], which are points p and q respectively
- Direction 3 is the cross product of direction 1 and the vector through points p and q
- Direction 2 is the cross product of directions 1 and 3

Using the I-J-K option you can define initial material directions that are aligned with the cells. This can be useful when modelling shapes such as cylinders where the principal directions are aligned with the major axes of the body.

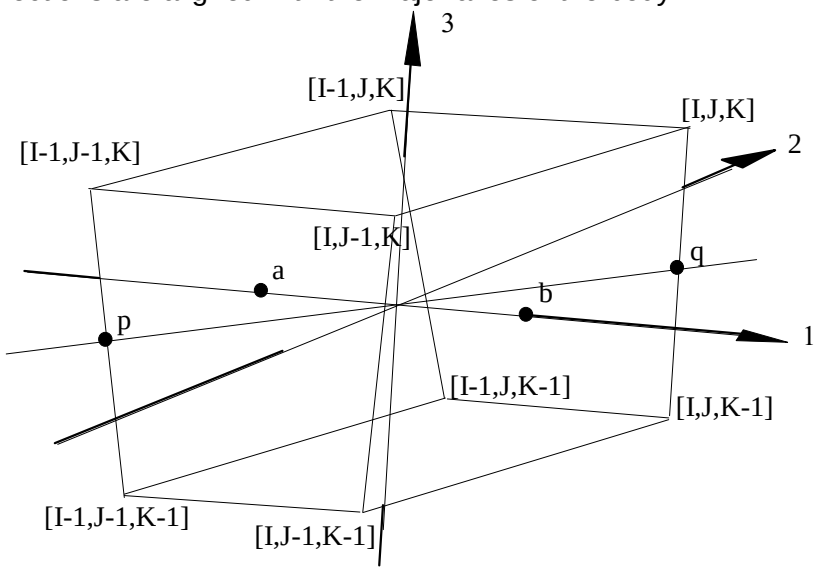

Figure 2-6 Material directions in AUTODYN-3D defined in IJK-space

3 Orthotropic Constitutive Models

In general the behaviour of composite laminates can be represented through a set of orthotropic constitutive relations. In Section 3.1 a set of such relationships are described which assume the material behaviour remains elastic and the volumetric response linear. For more complicated material response a methodology was developed, under contract from ESA (European Space Agency) [1], which allows a non-linear equation of state to be used in conjunction with an orthotropic stiffness matrix and is described in Section 3.2. This is important when modelling applications such as hypervelocity impacts.

Some composite materials, such as Kevlar-epoxy, exhibit significant non-linear stress-strain relationships, see Figure 3-1. In order to model such observed non-linear behaviour an orthotropic hardening model has been implemented. Again developed under contract from ESA [2] it uses an anisotropic plasticity based loading/failure surface and is described in Section 3.3.

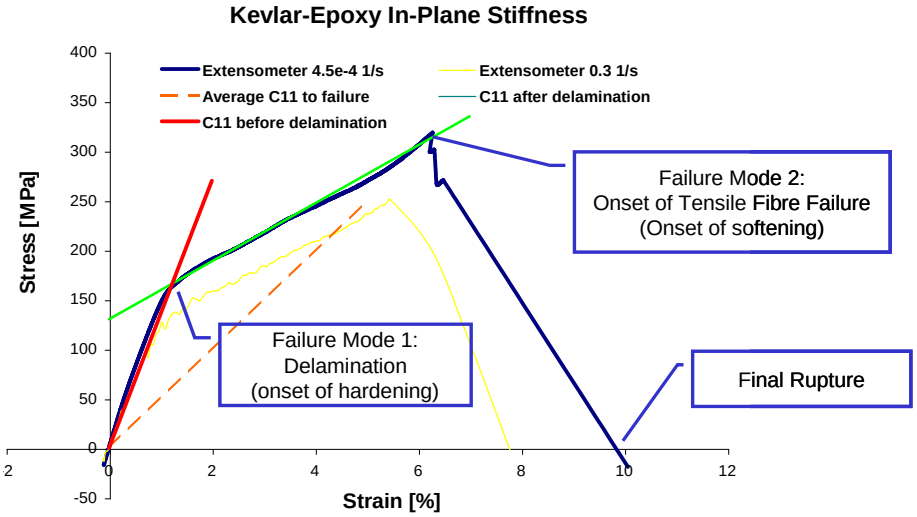

Figure 3-1 Typical in-plane stress-strain behaviour of Kevlar-epoxy

3.1 Orthotropic Elastic Model

For conventional materials the constitutive relations, or strength model, defines the deviatoric response of the material as a function of any combination of deviatoric strain, deviatoric strain rate, temperature, pressure, and damage.

$$C_{ij} = f\left(\varepsilon, \dot{\varepsilon}, T, P, D\right) \tag{3-1}$$

For many other materials, including composites, the macroscopic properties are not identical in all directions. In general, the behaviour of such materials is represented through a set of orthotropic constitutive relations. Constitutive relations for this type of material are conventionally based on a total stress formulation, as opposed to dividing the total stress into hydrostatic and deviatoric components. Thus, the incremental stress-strain relations can be expressed as

$$[\sigma]^{n+1} = [\sigma]^{n} + [C][\dot{\varepsilon}]\Delta t \tag{3-2}$$

where

[C]=stiffness matrix

$[\dot{\varepsilon}]$=strain rate tensor

Δt =time step.

The linear elastic constitutive relations for a general anisotropic (triclinic) material can be expressed in relation to a Cartesian co-ordinate system, in contracted notation, as

$$\begin{bmatrix}\sigma_{11}\\ \sigma_{22}\\ \sigma_{33}\\ \sigma_{23}\\ \sigma_{31}\\ \sigma_{12}\end{bmatrix} = \begin{bmatrix}C_{11} & C_{12} & C_{13} & C_{14} & C_{15} & C_{16}\\ C_{12} & C_{22} & C_{22} & C_{24} & C_{25} & C_{26}\\ C_{13} & C_{23} & C_{33} & C_{34} & C_{35} & C_{36}\\ C_{14} & C_{24} & C_{34} & C_{44} & C_{45} & C_{46}\\ C_{15} & C_{25} & C_{35} & C_{45} & C_{55} & C_{56}\\ C_{16} & C_{26} & C_{36} & C_{46} & C_{56} & C_{66}\end{bmatrix}\begin{bmatrix}\varepsilon_{11}\\ \varepsilon_{22}\\ \varepsilon_{33}\\ \varepsilon_{23}\\ \varepsilon_{31}\\ \varepsilon_{12}\end{bmatrix} \tag{3-3}$$

In which there are 21 independent elastic constants, C_{ij}. If there is one plane of material symmetry, the above stress strain relations reduce to

$$\begin{bmatrix}\sigma_{11}\\ \sigma_{22}\\ \sigma_{33}\\ \sigma_{23}\\ \sigma_{31}\\ \sigma_{12}\end{bmatrix} = \begin{bmatrix}C_{11} & C_{12} & C_{13} & 0 & 0 & C_{16}\\ C_{12} & C_{22} & C_{22} & 0 & 0 & C_{26}\\ C_{13} & C_{23} & C_{33} & 0 & 0 & C_{36}\\ 0 & 0 & 0 & C_{44} & C_{45} & 0\\ 0 & 0 & 0 & C_{45} & C_{55} & 0\\ C_{16} & C_{26} & C_{36} & 0 & 0 & C_{66}\end{bmatrix}\begin{bmatrix}\varepsilon_{11}\\ \varepsilon_{22}\\ \varepsilon_{33}\\ \varepsilon_{23}\\ \varepsilon_{31}\\ \varepsilon_{12}\end{bmatrix} \tag{3-4}$$

where the plane of symmetry is x_{33}=0. Such a material is termed monoclinic and there are 13 independent elastic constants. This is the basic form assumed for textiles and composites which generally have a plain of symmetry in the through thickness direction while the symmetry in the plane of the material is dependant on the lay-up and weave of the fibres.

If a second plane of symmetry exists in the plane of the fibre-composite then symmetry will also exist in a third mutually orthogonal plane. Such a material is said to be orthotropic and the constitutive relations are of the form:

$$\begin{bmatrix}\sigma_{11}\\ \sigma_{22}\\ \sigma_{33}\\ \sigma_{23}\\ \sigma_{31}\\ \sigma_{12}\end{bmatrix} = \begin{bmatrix}C_{11} & C_{12} & C_{13} & 0 & 0 & 0\\ C_{12} & C_{22} & C_{22} & 0 & 0 & 0\\ C_{13} & C_{23} & C_{33} & 0 & 0 & 0\\ 0 & 0 & 0 & C_{44} & 0 & 0\\ 0 & 0 & 0 & 0 & C_{55} & 0\\ 0 & 0 & 0 & 0 & 0 & C_{66}\end{bmatrix}\begin{bmatrix}\varepsilon_{11}\\ \varepsilon_{22}\\ \varepsilon_{33}\\ \varepsilon_{23}\\ \varepsilon_{31}\\ \varepsilon_{12}\end{bmatrix} \tag{3-5}$$

The inverse of the above stiffness matrix for a three-dimensional orthotropic configuration, the compliance matrix, is

$$[S]=\begin{bmatrix} \frac{1}{E_{11}} & \frac{-\upsilon_{12}}{E_{11}} & \frac{-\upsilon_{31}}{E_{33}} & 0 & 0 & 0 \\ \frac{-\upsilon_{12}}{E_{11}} & \frac{1}{E_{22}} & \frac{-\upsilon_{23}}{E_{22}} & 0 & 0 & 0 \\ \frac{-\upsilon_{31}}{E_{33}} & \frac{-\upsilon_{23}}{E_{22}} & \frac{1}{E_{33}} & 0 & 0 & 0 \\ 0 & 0 & 0 & \frac{1}{2G_{23}} & 0 & 0 \\ 0 & 0 & 0 & 0 & \frac{1}{2G_{31}} & 0 \\ 0 & 0 & 0 & 0 & 0 & \frac{1}{2G_{12}} \end{bmatrix} \quad (3\text{-}6)$$

where,

E_{ii} are the Young's Moduli in the principal material directions,
G_{ij} are the shear moduli,
ν_{ij} are the Poisson's ratios, where υ_{ij} is defined as the transverse strain in the j-direction when stressed in the i-direction, that is:

$$\upsilon_{ij} = -\frac{\varepsilon_j}{\varepsilon_i}, \quad \text{note that} \quad \upsilon_{ij} = \upsilon_{ji} * \frac{E_{ii}}{E_{jj}}.$$

Note that in AUTODYN-2D the directions 23 and 31 do not apply, so:

G_{23} and G_{31} are not required

$\dot{\varepsilon}_{23} = \dot{\varepsilon}_{31} = 0$

$\sigma_{23} = \sigma_{31} = 0$

The above, and similar, constitutive relations for orthotropic materials are commonly applied to fibre reinforced composites in which the fibres are set in a solid matrix material. Inherent in the model is the assumption of a linear volumetric elastic response of the material. This may not be representative of actual material response under the high pressures experienced during a hypervelocity impact event.

There are, of course, restrictions on the elastic constants that can be used for an orthotropic material and these restrictions are more complex than those for isotropic materials. These restrictions result from the fact that the sum of work done by all stress components must be positive in order to avoid the creation of energy. The first condition states that the elastic constants are positive:

$$E_{11}, E_{22}, E_{33}, G_{12}, G_{23}, G_{31} > 0 \quad (3\text{-}7)$$

Secondly the determinant of the stiffness matrix should be positive:

$$\Delta = 1 - \upsilon_{12}\upsilon_{21} - \upsilon_{31}\upsilon_{13} - \upsilon_{23}\upsilon_{32} - 2\upsilon_{21}\upsilon_{32}\upsilon_{13} > 0 \quad (3\text{-}8)$$

Finally the requirement for positive stiffnesses leads to:

$$\upsilon_{21} < \sqrt{\left[\frac{E_{22}}{E_{11}}\right]}, \quad \upsilon_{32} < \sqrt{\left[\frac{E_{33}}{E_{22}}\right]}, \quad \upsilon_{13} < \sqrt{\left[\frac{E_{11}}{E_{33}}\right]} \quad (3\text{-}9)$$

Whenever the elastic constants in an AUTODYN model are defined or redefined the three conditions above are tested and the user is informed if any of them are violated.

3.2 Equations of State

The material model developed in [1] provides a mechanism in an orthotropic material to calculate:

- The contributions to pressure from the isotropic and deviatoric strain components
- The contributions to the deviatoric stress from the deviatoric strains

Further, this methodology gives rise to the possibility for incorporating non-linear effects (such as shock effects) that can be attributed to the volumetric straining in the material. To use this model 'Ortho' is selected as the equation state for the material and either 'Polynomial' or 'Shock' for the volumetric response option.

The incremental linear elastic constitutive relations for an orthotropic material can be expressed, in contracted notation, as:

$$\begin{bmatrix} \Delta\sigma_{11} \\ \Delta\sigma_{22} \\ \Delta\sigma_{33} \\ \Delta\sigma_{23} \\ \Delta\sigma_{31} \\ \Delta\sigma_{12} \end{bmatrix} = \begin{bmatrix} C_{11} & C_{12} & C_{13} & 0 & 0 & 0 \\ C_{12} & C_{22} & C_{22} & 0 & 0 & 0 \\ C_{13} & C_{23} & C_{33} & 0 & 0 & 0 \\ 0 & 0 & 0 & C_{44} & 0 & 0 \\ 0 & 0 & 0 & 0 & C_{55} & 0 \\ 0 & 0 & 0 & 0 & 0 & C_{66} \end{bmatrix} \begin{bmatrix} \Delta\varepsilon_{11} \\ \Delta\varepsilon_{22} \\ \Delta\varepsilon_{33} \\ \Delta\varepsilon_{23} \\ \Delta\varepsilon_{31} \\ \Delta\varepsilon_{12} \end{bmatrix} \tag{3-10}$$

In order to include non-linear shock effects in the above linear relations, it is first desirable to separate the volumetric (thermodynamic) response of the material from its ability to carry shear loads (strength). To this end, it is convenient to split the strain increments into their average, $\Delta\varepsilon_{ave}$, and deviatoric, $\Delta\varepsilon_{ij}^{d}$, components.

$$\Delta\varepsilon_{ij} = \Delta\varepsilon_{ij}^{d} + \Delta\varepsilon_{ave} \tag{3-11}$$

Now, defining the average direct strain increment, $\Delta\varepsilon_{ave}$, as a third of the trace of the strain tensor,

$$\Delta\varepsilon_{ave} = \frac{1}{3}\left(\varepsilon_{11} + \varepsilon_{22} + \varepsilon_{33}\right) \tag{3-12}$$

and assuming, for small strain increments, the volumetric strain increment is defined as

$$\Delta\varepsilon_{vol} \approx \varepsilon_{11} + \varepsilon_{22} + \varepsilon_{33}. \tag{3-13}$$

The total strain increments can be expressed in terms of the volumetric and deviatoric strain increments resulting in the following orthotropic constitutive relation.

$$\begin{bmatrix}\Delta\sigma_{11}\\ \Delta\sigma_{22}\\ \Delta\sigma_{33}\\ \Delta\sigma_{23}\\ \Delta\sigma_{31}\\ \Delta\sigma_{12}\end{bmatrix}=\begin{bmatrix}C_{11} & C_{12} & C_{13} & 0 & 0 & 0\\ C_{12} & C_{22} & C_{22} & 0 & 0 & 0\\ C_{13} & C_{23} & C_{33} & 0 & 0 & 0\\ 0 & 0 & 0 & C_{44} & 0 & 0\\ 0 & 0 & 0 & 0 & C_{55} & 0\\ 0 & 0 & 0 & 0 & 0 & C_{66}\end{bmatrix}\begin{bmatrix}\Delta\varepsilon_{11}^{d}+\frac{1}{3}\Delta\varepsilon_{vol}\\ \Delta\varepsilon_{22}^{d}+\frac{1}{3}\Delta\varepsilon_{vol}\\ \Delta\varepsilon_{33}^{d}+\frac{1}{3}\Delta\varepsilon_{vol}\\ \Delta\varepsilon_{23}\\ \Delta\varepsilon_{31}\\ \Delta\varepsilon_{12}\end{bmatrix} \quad (3\text{-}14)$$

If the above relations are expanded and the deviatoric and volumetric terms grouped, the following expressions for the direct stress increments results.

$$\begin{aligned}\Delta\sigma_{11}&=\frac{1}{3}(C_{11}+C_{12}+C_{13})\Delta\varepsilon_{vol}+C_{11}\Delta\varepsilon_{11}^{d}+C_{12}\Delta\varepsilon_{22}^{d}+C_{13}\Delta\varepsilon_{33}^{d}\\ \Delta\sigma_{22}&=\frac{1}{3}(C_{21}+C_{22}+C_{23})\Delta\varepsilon_{vol}+C_{21}\Delta\varepsilon_{11}^{d}+C_{22}\Delta\varepsilon_{22}^{d}+C_{23}\Delta\varepsilon_{33}^{d}\\ \Delta\sigma_{33}&=\frac{1}{3}(C_{31}+C_{32}+C_{33})\Delta\varepsilon_{vol}+C_{31}\Delta\varepsilon_{11}^{d}+C_{32}\Delta\varepsilon_{22}^{d}+C_{33}\Delta\varepsilon_{33}^{d}\end{aligned} \quad (3\text{-}15)$$

To find the equivalent pressure increment, we first define the pressure as a third of the trace of the stress increment tensor;

$$\Delta P=-\frac{1}{3}(\Delta\sigma_{11}+\Delta\sigma_{22}+\Delta\sigma_{33}) \quad (3\text{-}16)$$

Substituting (3-15) into (3-16) results in an expression for the pressure increment of the form

$$\begin{aligned}\Delta P=\ &-\frac{1}{9}[C_{11}+C_{22}+C_{33}+2(C_{12}+C_{23}+C_{31})]\Delta\varepsilon_{vol}\\ &-\frac{1}{3}[C_{11}+C_{21}+C_{31}]\Delta\varepsilon_{11}^{d}\\ &-\frac{1}{3}[C_{12}+C_{22}+C_{32}]\Delta\varepsilon_{22}^{d}\\ &-\frac{1}{3}[C_{13}+C_{23}+C_{33}]\Delta\varepsilon_{33}^{d}\end{aligned} \quad (3\text{-}17)$$

from which the contributions to the pressure from volumetric and deviatoric components of strain can clearly be identified.

For an isotropic material, the stiffness matrix coefficients can be represented in terms of the material bulk modulus, K, and shear modulus, G. Thus,

$$\begin{aligned}C_{11}=C_{22}=C_{33}&=K+\frac{4}{3}G\\ C_{12}=C_{21}=C_{23}=C_{32}=C_{31}=C_{13}&=K-\frac{2}{3}G\end{aligned} \quad . \quad (3\text{-}18)$$

Substituting (3-18) into (3-16) gives

$$\Delta P=-K\Delta\varepsilon_{vol}-K(\Delta\varepsilon_{11}^{d}+\Delta\varepsilon_{22}^{d}+\Delta\varepsilon_{33}^{d}) \quad (3\text{-}19)$$

and given

$$\Delta\varepsilon_{11}^{d} + \Delta\varepsilon_{22}^{d} + \Delta\varepsilon_{33}^{d} = 0 \tag{3-20}$$

(3-19) reduces to

$$\Delta P = -K\Delta\varepsilon_{vol} \tag{3-21}$$

which is immediately recognisable as the standard relationship between pressure and volumetric strain (Hooke's law) at low compressions.

The first term of (3-17) can therefore be used to define the volumetric (thermodynamic) response of an orthotropic material in which the effective bulk modulus of the material K' is

$$K' = \frac{1}{9}\left[C_{11} + C_{22} + C_{33} + 2\left(C_{12} + C_{23} + C_{31}\right)\right]. \tag{3-22}$$

For the inclusion of non-linear shock effects, the contribution to pressure from volumetric strain is modified to include non-linear terms. The final incremental pressure calculation becomes

$$\begin{aligned} \Delta P = \quad & \Delta P_{EOS}\left(\varepsilon_{vol}, e\right) \\ & -\frac{1}{3}\left[C_{11} + C_{21} + C_{31}\right]\Delta\varepsilon_{11}^{d} \\ & -\frac{1}{3}\left[C_{12} + C_{22} + C_{32}\right]\Delta\varepsilon_{22}^{d} \\ & -\frac{1}{3}\left[C_{13} + C_{23} + C_{33}\right]\Delta\varepsilon_{33}^{d} \end{aligned} \tag{3-23}$$

where the pressure contribution ΔP_{EOS} from volumetric strains can include the non-linear shock (thermodynamic) effects and energy dependence as in a conventional equation of state.

A form of equation of state that is used extensively for isotropic solid continua is known as the Mie-Grüneisen form:

$$p = p_r\left(v\right) + \frac{\Gamma\left(v\right)}{v}\left[e - e_r\left(v\right)\right] \tag{3-24}$$

Where the Grüneisen gamma is defined as

$$\Gamma\left(v\right) = v\left(\frac{\partial p}{\partial e}\right)_v \tag{3-25}$$

The functions $p_r(v)$ and $e_r(v)$ are assumed to be known functions of v on some reference curve.

Two Mie-Grüneisen forms of equation of state are available for coupling with an orthotropic response in the AMMHIS model and are now described.

3.2.1 Shock Equation of State

To define the pressure and energy on the Hugoniot this equation of state requires the material shock velocity-particle velocity relationship as material input. In AUTODYN this is specified through

$$U_s = C_0 + Su_p \tag{3-26}$$

where,

U_s is the shock velocity,
U_p is the particle velocity,
S is the slope of the Us-up relationship,
C_o is the bulk acoustic sound speed.

For the case of an orthotropic material, the bulk acoustic sound speed is calculated from the effective bulk modulus (3-22) and density:

$$C_0 = \sqrt{\frac{K'}{\rho}} \tag{3-27}$$

3.2.2 Polynomial Equation of State

This is of the form

$$P = K'\varepsilon_{vol} + A_2(\varepsilon_{vol})^2 + A_3(\varepsilon_{vol})^3 + (B_0 + B_1\varepsilon_{vol})\rho_0 e \tag{3-28}$$

where the first term in (3-28) is equivalent to a linear equation of state with the bulk modulus, K', derived from the orthotropic material stiffness coefficients.

3.3 Strength and Hardening Model

In this section we describe in detail the implementation of a quadratic limit surface used to model the anisotropic hardening behaviour observed in some composite materials.

There are perhaps two definitions for failure; for a structural designer failure may be considered the point at which the material starts to become non-linear (due to plasticity or micro-cracking etc.), however for the simulation of extreme loading events such as HVI failure is considered to be the point at which the material actually ruptures (becomes perforated). To get to this point, the material transitions elastic to in-elastic deformation (due to micro-cracking, plasticity in the matrix or re-orientation of fibres) and finally reaches ultimate failure. We take the later definition, and for the purposes of this model we will term this non-linear stress strain behaviour “hardening”, see Figure 3-1.

The anisotropic yield criteria of Tsai-Hill can be used to represent the potentially different limits in elastic material behaviour in the three orthotropic material directions [5]. This type of surface is often used to model anisotropic yielding in materials with isotropic stiffness such as metals and polymers. This method does however have some limitations for materials with orthotropic stiffness. The first is that it is assumed that all inelastic deformation is at constant volume, i.e. due to deviatoric strain. However, for anisotropic materials, deviatoric strain contributes to the volumetric pressure. Hence it may be inconsistent to not change the volume (and therefore pressure) when inelastic deformation takes place. The model also does not include any hardening, the yield/initial failure surface remains at a constant level of stress.

A nine-parameter yield function was presented by Chen et al [3] and has been implemented into the AUTODYN code [2]. This model relaxes the constant pressure assumption in Hill’s theory and therefore is more generally applicable to materials with orthotropic stiffness. With careful selection of the parameters one can however return to the constant volume assumption. The yield function also includes a

hardening parameter. Softening behaviour and damage is not included with this yield function but it should be generally applicable to fibre reinforced composite materials. Also, because of the generality of the yield function it is applicable to both isotropic and anisotropic materials. The additional benefit of using a plasticity based hardening approach is that it can be used in conjunction with the existing non-linear shock response features described in Section 3.2.

3.3.1 Quadratic Limit Surface

The quadratic yield/flow surface [3] was selected to represent non-linear hardening effects.

$$\begin{aligned} f(\sigma_{ij}) = {} & a_{11}\sigma_{11}^2 + a_{22}\sigma_{22}^2 + a_{33}\sigma_{33}^2 + 2a_{12}\sigma_{11}\sigma_{22} + \\ & 2a_{23}\sigma_{22}\sigma_{33} + 2a_{13}\sigma_{11}\sigma_{33} + 2a_{44}\sigma_{23}^2 + \\ & 2a_{55}\sigma_{31}^2 + 2a_{66}\sigma_{12}^2 = k \end{aligned} \tag{3-29}$$

The yield function is quadratic in material stress space and includes nine material constants, a_{ij}, to represent the degree of anisotropy in the material behaviour. The parameter K varies with the effective inelastic strain in the material and can be used to represent hardening behaviour.

This yield surface is very general and by careful selection of the coefficients a_{ij} can reduce to several other well-known yield criteria. The yield criteria (3-29) reduces to Hill's orthotropic yield function under the following conditions:

$$\begin{aligned} a_{12} &= a_{33} - (a_{11} + a_{22} + a_{33})/2 \\ a_{13} &= a_{22} - (a_{11} + a_{22} + a_{33})/2 \\ a_{23} &= a_{11} - (a_{11} + a_{22} + a_{33})/2 \end{aligned} \tag{3-30}$$

Also, the von Mises J_2 yield criteria is recovered if the following values are set for the a_{ij} plasticity parameters:

$$\begin{aligned} a_{11} &= a_{11} = a_{11} = 2/3 \\ a_{12} &= a_{23} = a_{13} = -1/3 \\ a_{44} &= a_{55} = a_{66} = 1 \end{aligned} \tag{3-31}$$

The plasticity parameters would ideally be calibrated from the experimental stress-strain data obtained from three simple uniaxial tension tests and three pure shear tests. The six parameters associated with the normal stresses are then determined from the definition of a master effective stress-effective plastic strain $\left(\overline{\sigma} - \overline{\varepsilon}^p\right)$ relationship and from the definition of Plastic Poisson's' ratios (PPR). The three constants associated with the shear stresses are then obtained by collapsing the corresponding data onto the $\overline{\sigma} - \overline{\varepsilon}^p$ curve. In practice all the necessary stress-strain data are not usually available and assumptions have to be made. Indeed in [3] the required stress-strain data was obtained by 3D micro mechanical simulations.

It is necessary that the plasticity parameters, A11 to A66, define a real closed surface in stress space. To ensure this requirement is met the following constraints are placed on the plasticity parameters,

A_{11}, A_{22}, A_{33}, A_{44}, A_{55} & $A_{66} > 0$.

Additionally, the following two matrices are defined,

$$E = \begin{bmatrix} A_{11} & A_{12} & A_{13} & 0 \\ A_{12} & A_{22} & A_{23} & 0 \\ A_{13} & A_{23} & A_{33} & 0 \\ 0 & 0 & 0 & -K \end{bmatrix} \quad , \qquad e = \begin{bmatrix} A_{11} & A_{12} & A_{13} \\ A_{12} & A_{22} & A_{23} \\ A_{13} & A_{23} & A_{33} \end{bmatrix}$$

where it is required that Det E < 0, and, the non-zero eigen values of the matrix e all have the same sign.

After initial yielding material behaviour will be partly elastic and partly plastic. In order to derive the relationship between the plastic strain increment and the stress increment it is necessary to make a further assumption about the material behaviour. The incremental plastic strains are defined as follows,

$$d\varepsilon_{ij}^{p} = d\lambda \frac{\partial f}{\partial \sigma_{ij}} \tag{3-32}$$

These are the Prandtl-Reuss equations, often called an associated flow rule, and state that the plastic strain increments are proportional to the stress gradient of the yield function. The proportionality constant, $d\lambda$, is known as the plastic strain-rate multiplier. Written out explicitly the plastic strain increments are given by

$$\begin{Bmatrix} d\varepsilon_{11}^{p} \\ d\varepsilon_{22}^{p} \\ d\varepsilon_{33}^{p} \\ d\varepsilon_{23}^{p} \\ d\varepsilon_{31}^{p} \\ d\varepsilon_{12}^{p} \end{Bmatrix} = \begin{Bmatrix} 2a_{11}\sigma_{11} + 2a_{12}\sigma_{22} + 2a_{13}\sigma_{33} \\ 2a_{12}\sigma_{11} + 2a_{22}\sigma_{22} + 2a_{23}\sigma_{33} \\ 2a_{13}\sigma_{11} + 2a_{23}\sigma_{22} + 2a_{33}\sigma_{33} \\ 4a_{44}\sigma_{23} \\ 4a_{55}\sigma_{31} \\ 4a_{66}\sigma_{12} \end{Bmatrix} d\lambda \tag{3-33}$$

PPR, ν_{ij}^{P} *, are defined as,*

$$\nu_{ij}^{P} = -\frac{d\varepsilon_{jj}^{P}}{d\varepsilon_{ii}^{P}}, \quad \text{(no summation over repeated indices)} \tag{3-34}$$

From (3-33) and (3-34) the following relationships are easily derived

$$\begin{aligned} &a_{11} = a_{22}\frac{\nu_{21}^{P}}{\nu_{12}^{P}} \quad , \quad a_{33} = a_{22}\frac{\nu_{23}^{P}}{\nu_{32}^{P}} \quad , \quad a_{11} = a_{33}\frac{\nu_{31}^{P}}{\nu_{13}^{P}} \\ &a_{12} = -a_{22}\nu_{21}^{P} \quad , \quad a_{23} = -a_{22}\nu_{23}^{P} \quad , \quad a_{13} = -a_{33}\nu_{31}^{P} \end{aligned} \tag{3-35}$$

The incremental effective plastic strain can be calculated through a concept of plastic work,

$$dW^{P} = \sigma_{ij}\, d\varepsilon_{ij}^{P} = \bar{\sigma}\, d\bar{\varepsilon}^{P} \tag{3-36}$$

We can rewrite (3-36) as,

$$\boldsymbol{\sigma}^{T} d\boldsymbol{\varepsilon}^{P} = \bar{\sigma}\, d\bar{\varepsilon}^{P} \tag{3-37}$$

If the plastic strain increment is replaced by the flow rule (3-32) and multiplied by the transpose of the stress tensor, and using the following definition of effective stress,

$$f = k = \frac{2}{3}\bar{\sigma}^2 \tag{3-38}$$

it is easily shown that the effective plastic strain increment for the quadratic yield function is,

$$\left(d\bar{\varepsilon}^P\right)^2 = \frac{8}{3} f\, d\lambda^2 \tag{3-39}$$

The following explicit definition of incremental effective plastic strain results from substitution of (3-29) into (3-39) and using (3-33)

$$\begin{aligned}\left(d\bar{\varepsilon}^P\right)^2 = \frac{2}{3\Delta}\Big\{&A_{11}\left(d\varepsilon_{11}^P\right)^2 + A_{22}\left(d\varepsilon_{22}^P\right)^2 + A_{33}\left(d\varepsilon_{33}^P\right)^2 \\ &+ 2A_{12}\, d\varepsilon_{11}^P\, d\varepsilon_{22}^P + 2A_{23}\, d\varepsilon_{22}^P\, d\varepsilon_{33}^P + 2A_{13}\, d\varepsilon_{11}^P\, d\varepsilon_{33}^P\Big\} \\ &+ \frac{4}{3}\left\{\frac{\left(d\varepsilon_{23}^P\right)^2}{a_{44}} + \frac{\left(d\varepsilon_{31}^P\right)^2}{a_{55}} + \frac{\left(d\varepsilon_{12}^P\right)^2}{a_{66}}\right\}\end{aligned} \tag{3-40}$$

where

$$\Delta = \begin{vmatrix} a_{11} & a_{12} & a_{13} \\ a_{12} & a_{22} & a_{23} \\ a_{13} & a_{23} & a_{33} \end{vmatrix}$$

and

$$A_{11} = a_{22}a_{33} - a_{23}^2 \quad , \quad A_{22} = a_{11}a_{33} - a_{13}^2 \quad , \quad A_{33} = a_{11}a_{22} - a_{13}^2$$
$$A_{12} = a_{13}a_{23} - a_{12}a_{33}, \quad A_{13} = a_{12}a_{23} - a_{13}a_{22}, \quad A_{23} = a_{12}a_{13} - a_{11}a_{23}$$

3.3.2 Stress Return Algorithm

The typical series of calculations that are carried out each incremental time step (or cycle) in an element are shown schematically in Figure 3-2. Starting at the bottom of Figure 3-2 the boundary and/or interactive forces are updated and combined with the forces for inner zones computed during the previous time cycle. Then, for all non-interactive nodes, the accelerations, velocities and positions are computed from the momentum equation and a further integration. From these values the new zone volumes and strain rates may be calculated. With the use of a material model together with the energy equation the zone pressures, stresses and energies may be calculated, thus providing forces for use at the start of the next integration cycle.

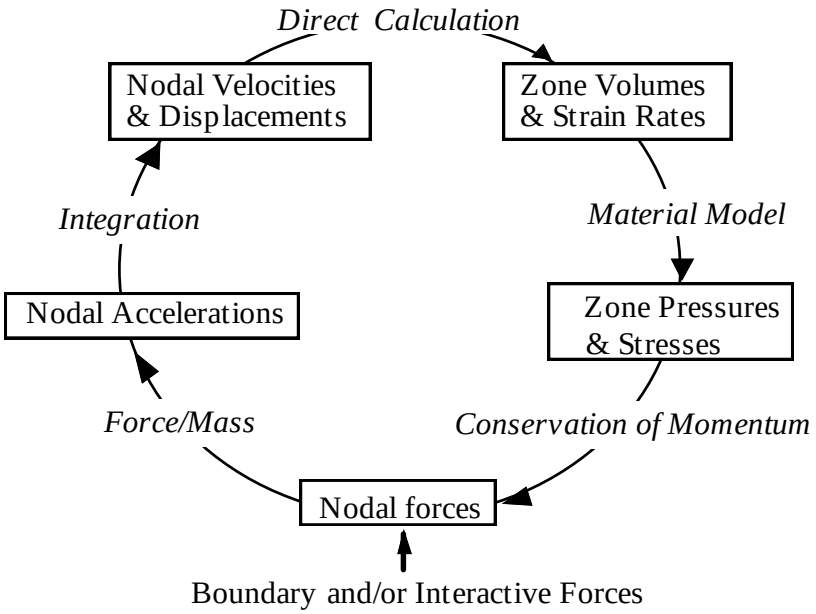

Figure 3-2 Computational Cycle

Having determined the strain rates and the volume change $\dot{V}/V$ the stresses can be calculated. These are then checked against the quadratic limit criteria of equation (3-29). Initially all stresses are updated using an elastic relationship. If these stresses remain within the yield surface then the material is assumed to have either loaded or unloaded elastically. If, however, the resultant updated stress state lies outside of the yield surface, point B in Figure 3-3, steps must be taken to return the stresses normal to the yield surface.

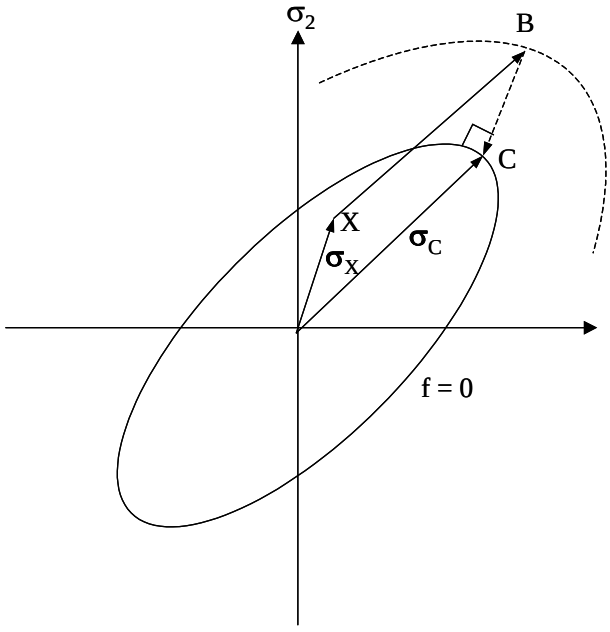

Figure 3-3 Yield surface

The backward-Euler stresses are calculated as,

$$\boldsymbol{\sigma}_C = \boldsymbol{\sigma}_B - \boldsymbol{C}\, d\boldsymbol{\varepsilon}^P \tag{3-41}$$

where, $\boldsymbol{C}$ is the elastic stiffness matrix and from the flow rule,

$$d\boldsymbol{\varepsilon}^P = \left.\frac{\partial f}{\partial \sigma_{ij}}\right|_{\boldsymbol{c}} d\lambda = \boldsymbol{a_c}\, d\lambda \tag{3-42}$$

which involves the vector $\boldsymbol{a}_c$ that is normal to the yield surface at the final position C. At this location the stress state satisfies the yield criteria. Except in special cases this vector $\boldsymbol{a}_c$ cannot be determined from the data at point B. Hence an iterative procedure must be used.

As a first step a predictor stress state, $\boldsymbol{\sigma}_C$ is calculated using the following equation,

$$\boldsymbol{\sigma}_C = \boldsymbol{\sigma}_B - d\lambda \boldsymbol{C a}_B \tag{3-43}$$

where,

$$d\lambda = \frac{f_B}{a_B^T C a_B} \tag{3-44}$$

$d\lambda$ here is defined so as to make the value of the yield function zero when a Taylor expansion of the yield criteria is performed about the trial point B. In general this will result in a stress state that still remains outside of the yield surface. This is because the normal at trial elastic state B is not equal to the final normal at point D, see Figure 3-4. Further iterations are therefore usually required.

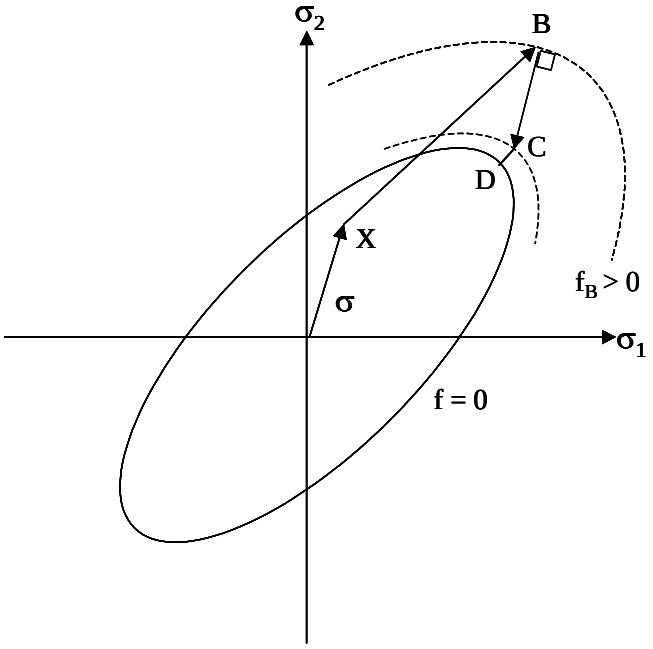

Figure 3-4 Schematic representation of backward-Euler return algorithm

The stress return is achieved using a backward-Euler return algorithm and the yield function is assumed to be satisfied if the returned stress state is within 1% of the yield surface.

Once the yield function is satisfied the plastic portion of the strain increment is determined from the following,

$$\left(d\bar{\varepsilon}^P\right)^2 = \frac{8}{3} f\, d\lambda^2 \tag{3-45}$$

4 Orthotropic Material Failure Models

4.1 Brittle Damage Model

For brittle materials, three orthotropic failure initiation models are available in AUTODYN-2D and 3D, as follows:

- Material Stress
- Material Strain
- Material Stress/Strain.

These models allow different tensile and shear failure stresses and/or strains for each of the principal (material) directions. The models are intended to enable modelling of orthotropic failure.

Importantly, the orthotropic failure models can be used together with the orthotropic equation of state, which before failure uses the incremental elastic stress-strain relations detailed in 3. With any of the above “Material” failure models, failure is initiated in a principal direction when the stress or strain reaches a user-specified limiting value.

4.1.1 Failure Initiation

Material Stress

This model is useful for materials that are likely to fail along predefined material planes: For instance, where delamination failure occurs between layers in a composite plate.

Tensile Failure Stress 11
Tensile Failure Stress 22
Tensile Failure Stress 33
Maximum Shear Stress 12
Maximum Shear Stress 23 (3D only)
Maximum Shear Stress 31 (3D only)

Failure is initiated if any of the principal material stresses exceed their respective tensile failure stresses. For shear failures the shear stress on planes parallel to the principal directions are checked against the maximum shear stress.

Material Strain

This model is useful for materials, which are likely to fail along predefined material planes: For instance, where failure occurs parallel to the interface between two layers in a laminated plate.

Tensile Failure Strain 11
Tensile Failure Strain 22
Tensile Failure Strain 33
Maximum Shear Strain 12
Maximum Shear Strain 23 (3D only)
Maximum Shear Strain 31 (3D only)

Failure is initiated if any of the principal material strains exceed their respective tensile failure strains. For shear failures the shear strain on planes parallel to the principal directions are checked against the maximum shear strain.

Mat.Stress/Strain
This model is useful for materials that are likely to fail along predefined material planes: For instance, where failure occurs, parallel to the interface, between two layers in a laminated plate.

Tensile Failure Stress 11
Tensile Failure Stress 22
Tensile Failure Stress 33
Maximum Shear Stress 12
Maximum Shear Stress 23 (3D only)
Maximum Shear Stress 31 (3D only)
Tensile Failure Strain 11
Tensile Failure Strain 22
Tensile Failure Strain 33
Maximum Shear Strain 12
Maximum Shear Strain 23 (3D only)
Maximum Shear Strain 31 (3D only)

Failure is initiated if any of the principal material stresses or strains exceed their respective failure levels. For shear failures the shear stresses, and strains, on planes parallel to the principal directions are checked against the inputted maximum shear stresses, and strains.

4.1.2 Post-Failure Response

When an orthotropic equation of state is used in conjunction with material stress, strain or stress/strain failure criteria an option to use isotropic or orthotropic post failure response is included in the failure data input. Subsequent to failure initiation, the failed cell stiffness and strength properties are modified depending on the failure initiation modes described in the subsections below.

4.1.2.1 *Isotropic Post-Failure*

The failure models outlined in Section 4.1.1 allow different tensile and shear failure stresses and/or strains for each of the “principal” directions. If the isotropic post-failure option is selected failed cells can only carry bulk compressive stresses. Therefore after failure is initiated in a cell the following occurs:

- The principal (material) stress in the direction of failure is set to zero.
- All shear modulii are set to zero
- All shear stresses are set to zero
- The average stress (i.e. pressure) is recomputed, using the normal calculation:

$$P = -\frac{1}{3}\left(\sigma_{11} + \sigma_{22} + \sigma_{33}\right)$$

For the orthotropic equation of state, post-failure behaviour is modelled as detailed below. This post-failure model is in effect an isotropic post-failure response.

- The orthotropic elastic incremental stress-strain relations are applied.
- The average stress (i.e. pressure) is recomputed, using the calculation above.
- If the cell is in compression,
  The principal stresses are set equal to the average stress (i.e. pressure):
  $$\sigma_{ii} = -P$$
- If the cell is in tension,
  All principal stresses, and therefore the average stress (i.e. pressure), are set to zero: $\sigma_{ii} = -P = 0$

4.1.2.2 *Orthotropic Post-Failure Response*

The post-failure behaviour of laminated composite materials is better represented through the orthotropic post failure option. This option was developed specifically for simulating the performance and failure, including delamination, of fibre reinforced composite materials.

If the orthotropic option is selected, the user is prompted to define the post-failure parameters. This includes the post failure response mode for failure in each material direction and the failed material residual shear strength, see Table 4-1:

Failed Direction	Post Failure Option	Post Failure Response
FAIL 11	11 only Bulk	Zero tensile stress in 11 direction Zero tensile stress in all directions
FAIL 22	22 only Bulk	Zero tensile stress in 22 direction Zero tensile stress in all directions
FAIL 33	33 only Bulk	Zero tensile stress in 33 direction Zero tensile stress in all directions
FAIL 12	12 & 11 only 12 & 22 only Bulk	Zero tensile stress in 11 direction Zero tensile stress in 22 direction Zero tensile stress in all directions
Residual Shear Stiffness Frac.	0.0 to 1.0	Residual shear modulus is set to the specified value times the intact shear modulus. Default value is 0.2
Max. Resid. Shear Stress	0.0 to 1.0e20	Maximum shear stress allowed in a failed cell. A value equal to, or less than, the failure shear stress is recommended.

Table 4-1 Orthotropic post-failure options

For all failure modes, on failure initiation, the stress in the failed material directions are set to zero. In addition the stresses in material directions orthogonal to the failed direction are reduced to account for the loss in the Poisson effect from strain in the failed direction. In subsequent cycles, cell tensile stresses are only allowed in non-failed directions.

If a cell fails in two or more directions, bulk failure is assumed.

Subsequent to failure initiation, the failed cell stiffness and strength properties are modified depending on the failure initiation modes described in the subsections below.

4.1.2.2.1 Delamination

In an axisymmetric simulation, the 11-direction is assumed to be through the thickness of the laminate and the 33-direction is the hoop direction. Delamination can result from excessive through thickness tensile stresses and/or strains or from excessive shear stress and or strain in the 12 plane. If failure is initiated in either of these two modes, the stress in the 11-direction is instantaneously set to zero and the strain in the 11-direction at failure is stored. Subsequently, if the tensile material strain in the 11-direction exceeds the failure strain, the material stiffness matrix is modified as

$$\begin{bmatrix} 0 \\ \Delta\sigma_{22} \\ \Delta\sigma_{33} \\ \Delta\sigma_{23} \\ \Delta\sigma_{31} \\ \Delta\sigma_{12} \end{bmatrix} = \begin{bmatrix} 0 & 0 & 0 & 0 & 0 & 0 \\ 0 & C_{22} & C_{22} & 0 & 0 & 0 \\ 0 & C_{23} & C_{33} & 0 & 0 & 0 \\ 0 & 0 & 0 & \alpha C_{44} & 0 & 0 \\ 0 & 0 & 0 & 0 & \alpha C_{55} & 0 \\ 0 & 0 & 0 & 0 & 0 & \alpha C_{66} \end{bmatrix} \begin{bmatrix} \Delta\varepsilon_{11} \\ \Delta\varepsilon_{22} \\ \Delta\varepsilon_{33} \\ \Delta\varepsilon_{23} \\ \Delta\varepsilon_{31} \\ \Delta\varepsilon_{12} \end{bmatrix} \quad (4\text{-}1)$$

This stiffness modification does not allow tensile through thickness stresses while tensile in-plane stresses are maintained.

Also note that the delamination will in practice be associated with a reduction in shear stiffness. Often, in the absence of appropriate material data, a nominal value of 20% is typically used for the residual shear stiffness α.

4.1.2.2.2 In-plane Failure

In an axisymmetric simulation, the 22- and 33-directions are assumed to be in the plane of the composite i.e. in the fibre directions. If failure is initiated in these two modes, the stress in the failed direction is instantaneously set to zero and the strain in the failed direction at failure is stored. Subsequently, if the tensile material strain in the failed direction exceeds the failure strain, the material stiffness matrix is modified as

22-failure:

$$\begin{bmatrix} \Delta\sigma_{11} \\ 0 \\ \Delta\sigma_{33} \\ \Delta\sigma_{23} \\ \Delta\sigma_{31} \\ \Delta\sigma_{12} \end{bmatrix} = \begin{bmatrix} C_{11} & 0 & C_{13} & 0 & 0 & 0 \\ 0 & 0 & 0 & 0 & 0 & 0 \\ C_{13} & 0 & C_{33} & 0 & 0 & 0 \\ 0 & 0 & 0 & \alpha C_{44} & 0 & 0 \\ 0 & 0 & 0 & 0 & \alpha C_{55} & 0 \\ 0 & 0 & 0 & 0 & 0 & \alpha C_{66} \end{bmatrix} \begin{bmatrix} \Delta\varepsilon_{11} \\ \Delta\varepsilon_{22} \\ \Delta\varepsilon_{33} \\ \Delta\varepsilon_{23} \\ \Delta\varepsilon_{31} \\ \Delta\varepsilon_{12} \end{bmatrix} \quad (4\text{-}2)$$

33-failure:

$$\begin{bmatrix} \Delta\sigma_{11} \\ \Delta\sigma_{22} \\ 0 \\ \Delta\sigma_{23} \\ \Delta\sigma_{31} \\ \Delta\sigma_{12} \end{bmatrix} = \begin{bmatrix} C_{11} & C_{12} & 0 & 0 & 0 & 0 \\ C_{12} & C_{22} & 0 & 0 & 0 & 0 \\ 0 & 0 & 0 & 0 & 0 & 0 \\ 0 & 0 & 0 & \alpha C_{44} & 0 & 0 \\ 0 & 0 & 0 & 0 & \alpha C_{55} & 0 \\ 0 & 0 & 0 & 0 & 0 & \alpha C_{66} \end{bmatrix} \begin{bmatrix} \Delta\varepsilon_{11} \\ \Delta\varepsilon_{22} \\ \Delta\varepsilon_{33} \\ \Delta\varepsilon_{23} \\ \Delta\varepsilon_{31} \\ \Delta\varepsilon_{12} \end{bmatrix} \quad (4\text{-}3)$$

This stiffness modification does not allow tensile stresses in the failed directions. Also note that these failure modes will in practice be associated with a reduction in shear stiffness. Often, in the absence of appropriate material data, a nominal value of 20% is typically used for the residual shear stiffness α.

4.1.2.2.3 Combined Failure

The combined effect of failure in all three material directions is represented by a change in the material stiffness and strength to isotropic with no stress deviators and no tensile material stresses.

4.1.2.2.4 Melting and Decomposition

Melting/vaporisation of epoxy and decomposition of the fibre material has been observed in composites with an epoxy matrix, for example Kevlar-epoxy [1]. This occurred in a finite region directly under the impact point under uniaxial strain conditions and velocities above or around 1000m/s

To represent this phenomena in an approximate way in a numerical model, the following features are available. An epoxy melting temperature can be specified. It is assumed that this has a very similar effect to delamination in the laminate. The procedure outlined in Section 4.1.2.2.1 is followed for this failure initiation mode.

Additionally, a decomposition temperature for the fibre can be specified. Decomposition may lead to an inhomogeneous material of unknown properties. The model therefore assumes that the decomposed material has properties of the intact material under bulk compression. In bulk tension, pressure, deviatoric and tensile stresses are set to zero.

4.2 Orthotropic Damage Model

Composite materials are not perfectly brittle, instantaneous failure is not necessarily observed in all or any of the material directions. The stress/strain based failure models available for use in conjunction with the orthotropic model instantaneously set material stresses to zero on failure initiation, as described in Section 4.1.

In this section we report developments [2] which model the softening behaviour observed in some composites, see Figure 3-1. Maximum tensile and shear stresses in a cell are limited by failure surfaces used to define failure initiation. Different failure modes are considered each of which are described by a unique surface. To model the gradual reduction in the ability of a laminate to carry stress a crack softening approach is used. This reduces the maximum tensile stress that can be sustained in an element as a function of some measure of crack strain.

4.2.1 Failure Initiation

Hashin failure criteria have been extensively used in modelling the prediction of impact damage in composites. However, in these criteria for fibre and matrix failure only plane stresses, $\sigma_{22,}$ σ_{23} and σ_{33}, are considered. As a consequence the applicability of these criteria for out of plane impacts is questionable.

Modified versions of these failure criteria along with a criterion for delamination are presented in [6] and have been implemented into AUTODYN [2]. For the fibre failure and matrix cracking criteria out of plane shear stresses are included in addition to the original criteria. The failure initiation criteria are listed below.

11-plane $$e_{11f}^2 = \left(\frac{\sigma_{11}}{\sigma_{11fail}}\right)^2 + \left(\frac{\sigma_{12}}{\sigma_{12fail}}\right)^2 + \left(\frac{\sigma_{31}}{\sigma_{31fail}}\right)^2 \geq 1 \qquad (4\text{-}4)$$

22-plane $$e_{22f}^2 = \left(\frac{\sigma_{22}}{\sigma_{22fail}}\right)^2 + \left(\frac{\sigma_{12}}{\sigma_{12fail}}\right)^2 + \left(\frac{\sigma_{23}}{\sigma_{23fail}}\right)^2 \geq 1 \qquad (4\text{-}5)$$

33-plane $$e_{33f}^2 = \left(\frac{\sigma_{33}}{\sigma_{33fail}}\right)^2 + \left(\frac{\sigma_{23}}{\sigma_{23fail}}\right)^2 + \left(\frac{\sigma_{31}}{\sigma_{31fail}}\right)^2 \geq 1 \qquad (4\text{-}6)$$

The initiation criteria (4-4) to (4-6) are only applied in tension.

4.2.2 Damage Model

The failure initiation criteria can be considered as surfaces that define regions of valid stress. If a state of stress is found to lay outside of this surface a backward-Euler algorithm is used to return the stress to the failure surface. The resulting inelastic increment in strain is then accumulated as crack strain ε_{cr}. The maximum stress that can be sustained in an element is then reduced as a function of crack strain.

In this approach the area under the softening portion of the stress/strain curve is related to the fracture energy G_f, which is a material property. This is simply illustrated in Figure 4-1.

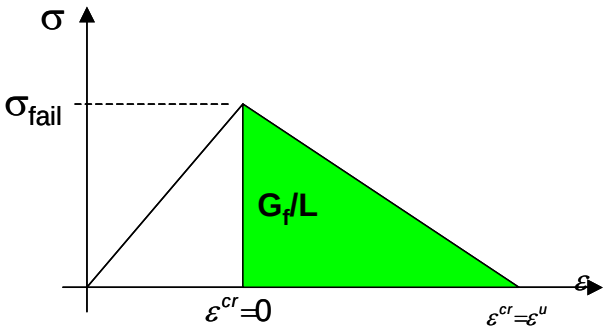

Figure 4-1 Schematic illustration of crack softening algorithm

A mathematical description of Figure 4-1 can be written as,

$$G_f = \int_{\varepsilon^{cr}=0}^{\varepsilon^{cr}=\varepsilon^u} \sigma L \, d\varepsilon^{cr} \qquad (4\text{-}7)$$

where L is a characteristic cell dimension in the direction of failure and is included to improve the objectivity of the solution.

Failure is initiated when the stress reaches the value required for failure σ_{fail}. At this point the crack strain ε_{cr} is zero. A linear softening slope is assumed and therefore the ultimate crack strain ε^U, the strain at which tensile stresses can no longer be sustained, is calculated as:

$$\varepsilon^u = \frac{2G_f}{\sigma_{fail} L} \qquad (4\text{-}8)$$

The gradient of the linear softening slope is given by:

$$h = \frac{L\sigma_{fail}^2}{2G_f} \tag{4-9}$$

After failure initiation a linear damage law is used to reduce the maximum material stress in a cell as a function of crack strain.

$$Dam = \frac{h \times \varepsilon^{cr}}{\sigma_{fail}} \tag{4-10}$$

At initiation ε_{cr} *=0* therefore *dam=0,* when the cell has no strength *dam=1*. At any point between these times the maximum tensile material stress that can be supported in the cell is:

$$\sigma_{\max} = \sigma_{fail}(1 - Dam) \tag{4-11}$$

Rather than define an effective crack strain analogous to effective plastic strain, damage has been implemented as a full tensor

$$\boldsymbol{\varepsilon}^{cr} = \begin{pmatrix} \varepsilon_{11}^{cr} \\ \varepsilon_{22}^{cr} \\ \varepsilon_{33}^{cr} \\ \varepsilon_{23}^{cr} \\ \varepsilon_{31}^{cr} \\ \varepsilon_{12}^{cr} \end{pmatrix} \tag{4-12}$$

Each component of (4-12) has an independent damage variable associated with it resulting in orthotropic damage. If we examine the 11-plane softening surface, damage is included for each stress component as follows,

$$e_{11f}^2 = \underbrace{\left(\frac{\sigma_{11}}{\sigma_{11fail}(1-D_{11})}\right)^2 + \left(\frac{\sigma_{12}}{\sigma_{12fail}(1-D_{12})}\right)^2 + \left(\frac{\sigma_{31}}{\sigma_{31fail}(1-D_{31})}\right)^2}_{\sigma_{eff}} \geq 1 \tag{4-13}$$

As with the hardening behaviour of 3.3 an associative flow rule is assumed when returning the stresses to the softening surfaces,

$$d\varepsilon_{ij}^{cr} = d\lambda \frac{\partial e}{\partial \sigma_{ij}} \tag{4-14}$$

Considering the flow rule (4-14) the incremental crack strain components are calculated as follows for the 11-plane softening surface (4-13),

$$d\boldsymbol{\varepsilon}^{cr} = \begin{pmatrix} d\varepsilon_{11}^{cr} \\ d\varepsilon_{22}^{cr} \\ d\varepsilon_{33}^{cr} \\ d\varepsilon_{23}^{cr} \\ d\varepsilon_{31}^{cr} \\ d\varepsilon_{12}^{cr} \end{pmatrix} = \frac{1}{\sigma_{eff}} \begin{Bmatrix} \sigma_{11} \Big/ \sigma_{11fail}^2 (1-D_{11})^2 \\ 0 \\ 0 \\ 0 \\ \sigma_{31} \Big/ \sigma_{31fail}^2 (1-D_{31})^2 \\ \sigma_{12} \Big/ \sigma_{12fail}^2 (1-D_{12})^2 \end{Bmatrix} \tag{4-15}$$

The possibility that an increase in damage in a particular direction may reduce the maximum strength in other directions can be incorporated via the damage coupling coefficient, *C*. The value of *C* can vary between 0 and 1. For example, for the failure surface considered above, the damage increments are updated as,

$$\Delta D_{11} = \frac{h_{11} \times \varepsilon_{11}^{cr}}{\sigma_{11fail}} + C\frac{h_{31} \times \varepsilon_{31}^{cr}}{\sigma_{31fail}} + C\frac{h_{12} \times \varepsilon_{12}^{cr}}{\sigma_{12fail}}$$

$$\Delta D_{31} = \frac{h_{31} \times \varepsilon_{31}^{cr}}{\sigma_{31fail}} + C\frac{h_{11} \times \varepsilon_{11}^{cr}}{\sigma_{11fail}} + C\frac{h_{12} \times \varepsilon_{12}^{cr}}{\sigma_{12fail}}$$

$$\Delta D_{12} = \frac{h_{12} \times \varepsilon_{12}^{cr}}{\sigma_{12fail}} + C\frac{h_{31} \times \varepsilon_{31}^{cr}}{\sigma_{31fail}} + C\frac{h_{11} \times \varepsilon_{11}^{cr}}{\sigma_{11fail}}$$

Similar equations are trivially derived for the other softening surfaces.

5 Material Characterisation Tests

To fully characterise a composite material requires an extensive series of experimental tests. The number of tests required though may vary depending on the material behaviour and the application. This section briefly describes experiments that have been used to obtain composite material properties for studies using the material models described in 3 and 4. The testing strategy described in this chapter has been developed under ESA research contract No. 12400/97/NL/PA(SC) and performed by Ernst Mach Institute (EMI), Freiburg, in conjunction with Century Dynamics, [1][2].

5.1 Directional Strength Properties

Normal in-plane testing of composites in compression and tension is standardised, for example standard EN ISO 527-4. Tensile and shear tests measure important material characteristics such as elastic and plastic Poisson ratios, non-linear hardening properties and failure limits and are now discussed.

5.1.1 In-Plane Tension Tests

5.1.1.1 *0° Tension Test*

Tensile tests are typically performed to determine the stress-strain response of a composite material in the plane of the laminate. Data commonly generated by this test are the stiffness and strength properties. Samples, of similar shape to that illustrated in Figure 5-1, are cut from the laminate sheets and the ends of the sample are clamped and separated at a constant speed in opposite directions using a machine such as an Instron®. The tension or force required to do this is recorded. The test results are shown as a stress-strain curve, the shape of which provides information about the material behaviour of the sample.

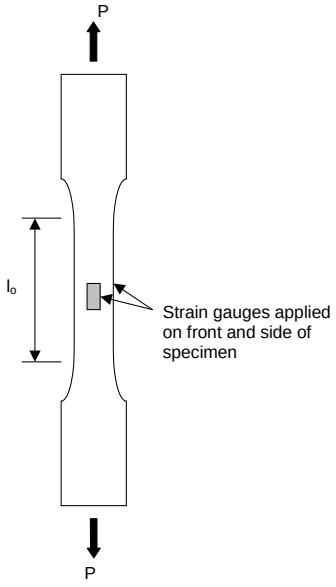

Figure 5-1 Schematic diagram of a Tensile Test specimen

Strains can be recorded by using the crosshead displacement of the experimental apparatus, or using an extensometer. Alternatively biaxial strain gauges located both on the side and front of the test specimen allow for measurement of the strains in the principal material directions. In this way both in-plane and through thickness properties can be measured. For unidirectional laminates, samples can be prepared

such that the specimens can be orientated either in the direction of the fibres (0° tension test) or at 90° to the fibres (90° tension test).

Figure 5-2 and
Figure 5-3 show a typical result of a tensile test on a composite material.

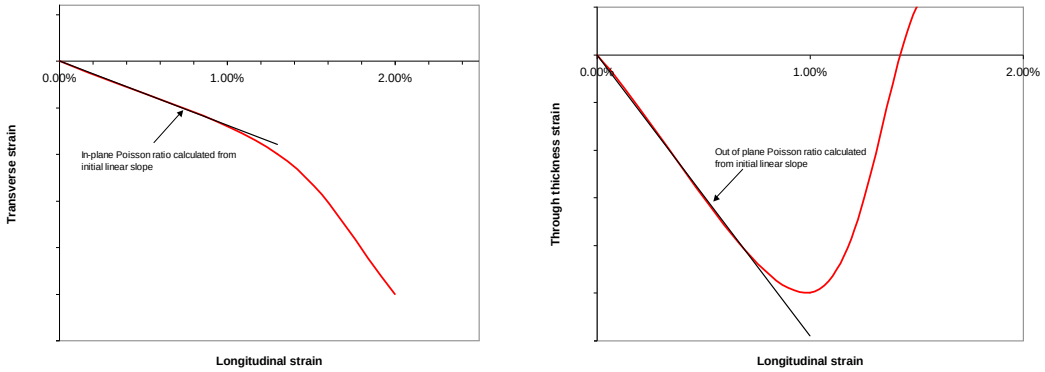

Figure 5-2 Calculation of in plane and out of plane Poisson ratios

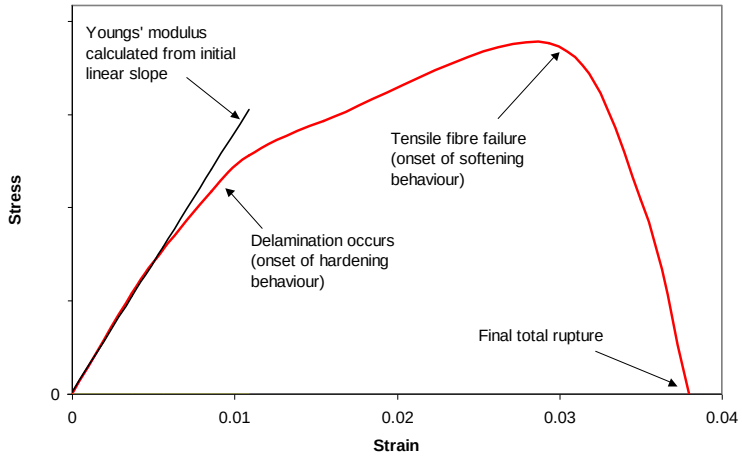

Figure 5-3 Typical recorded uniaxial stress-strain relationship

5.1.1.2 *45° Tension Test*

Tension tests on samples manufactured so that the fibres are aligned at 45° orientation to the applied load are performed to derive the in-plane shear modulus according to equation (5-1) [7]. Instrumentation with longitudinal and transverse strain gauges is applied as in the previous tests of Section 5.1.1.1.

$$G_{23} = \frac{1}{\left(\frac{4}{E_Y} - \frac{1}{E_{22}} - \frac{1}{E_{33}} + \frac{2\,\nu_{23}}{E_{22}} \right)} \qquad (5\text{-}1)$$

where E_y is the modulus calculated from the initial linear part of the recorded stress-strain relationship which in principal will have similar form to that shown in Figure 5-3.

5.1.2 Out-of-Plane Shear

The out-of-plane shear behaviour can be characterised by short beam shear experiments. Tests such as these, using either a three, four or five-point bending set-up, often suffer from the fact that significant bending is observed in the sample in addition to the shear deformation.

A test set-up developed at EMI, and used successfully in [2], minimises bending effects resulting in maximised shear deformation, see Figure 5-4. The shear force is recorded along with the total displacement using a clip gauge. The shear stress τ and the shear angle γ can then be derived. For full details of this experiment the reader is directed to [2].

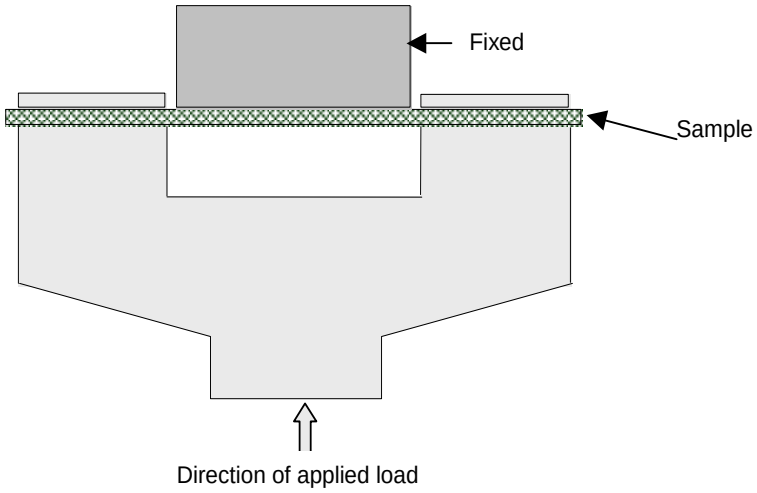

Figure 5-4 Short beam shear test setup

Figure 5-5 shows a typical the shear stress–shear strain relationship. The out of plane shear stiffness G_{13} and the matrix yielding stress τ_{matrix} is derived from the extensometer signals.

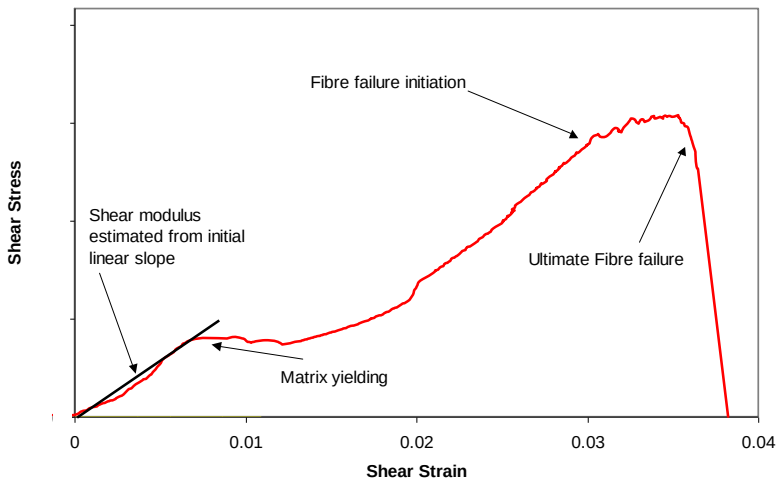

Figure 5-5 Typical Shear stress - shear angle relationship

5.2 Equation of State Properties

5.2.1 Inverse Flyer Plate Tests

Inverse planar plate experiments are used to obtain the uniaxial compression behaviour at strain rates up to 10^4/s. This method is very well adapted to characterise the shock compression behaviour of unknown materials. Studies have shown the importance of equation of state properties for accurate simulations of composite materials subjected to hypervelocity impact [1].

A schematic of the test is given in Figure 5-6. A projectile consisting of cylindrical samples of the composite being tested, covered typically with an Aluminium backing, are accelerated in a gas gun to velocities up to 1000 m/s. The projectile then impacts a stationary witness plate of well characterised steel. The velocity of the rear surface of the witness plate is recorded using a high resolution VISAR laser interferometer.

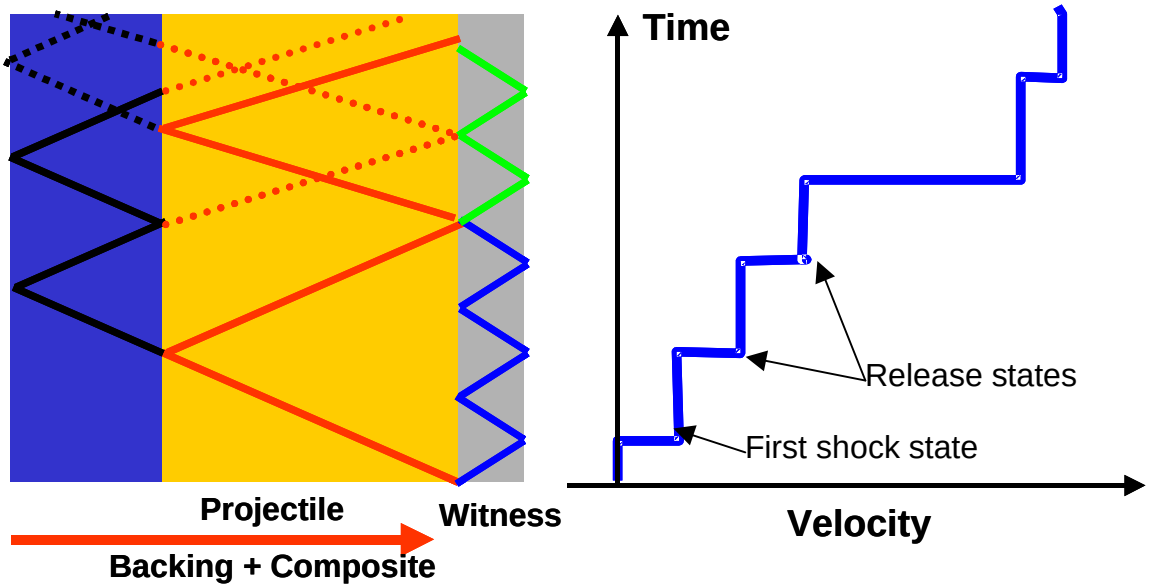

Figure 5-6 Configuration of inverse planar impact experiments and a typical velocity trace from the rear surface of the witness plate

Figure 5-6 shows a typical velocity trace for an inverse flyer plate experiment. After shocking the arriving material sample and the stationary witness plate on the contact surface to their respective Hugoniot states, the stress waves travel through both plates. The pressure wave inside the witness plate is converted to a pressure release wave at the free surface and propagates back into the steel. Due to the impedance mismatch between steel and the sample material, this wave is only partially transmitted across the impact surface into the sample. It is mainly converted back to a pressure wave, which provides a further velocity increase when reaching the free surface of the witness plate. The repeated reflection of the wave at the surfaces results in stepwise increase of the free surface velocity.

The complete impact conditions in the sample can be calculated without any assumption on the material's equation of state. Shock states are determined using the Rankine-Hugoniot equations, and the free surface velocity can be used to obtain the particle velocity, since the measured free surface velocity u_{fs} is approximately equal to twice the particle velocity u_p of the target at the first shock state of Figure

5-6. Together with the known shock properties of the target, the Rankine Hugoniot equations can be used to deduce all variables of the shock state. Further details of this experiment are given in [1][2].

5.3 Delamination Properties

In this section an overview of experimental techniques used to characterise delamination thresholds and energies are presented. A number of delamination modes are considered and are illustrated schematically in Figure 5-7.

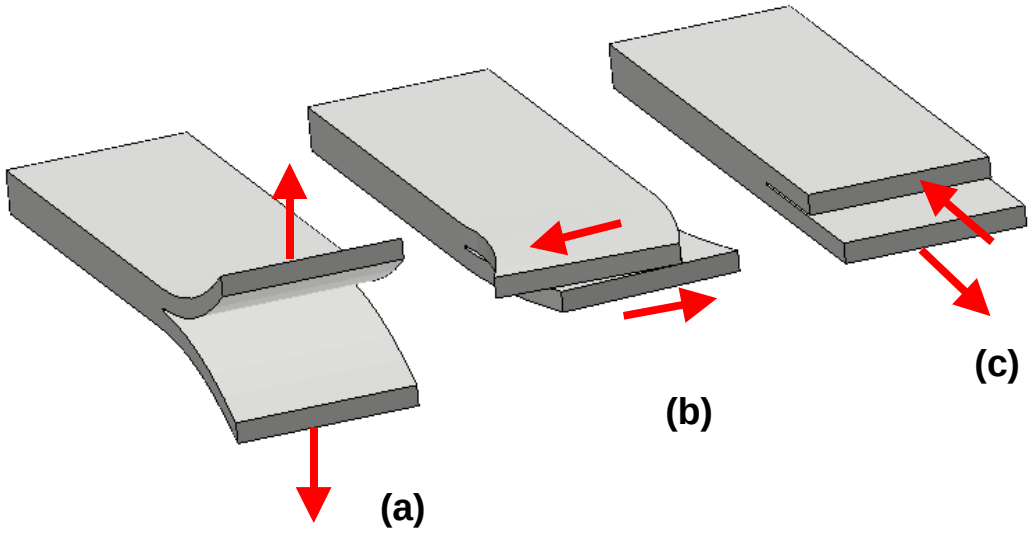

Figure 5-7 Delamination modes. (a) Mode I : Normal delamination. (b) Mode II : Shear delamination. (c) Mode III : Shear delamination

5.3.1 Direct Plate Impact - Mode I Delamination Strength

The through thickness strength at high strain rates can be determined by the use of a direct plate impact test. In this test the projectile and sample are designed in such a way as to ensure that release waves from the target free surface and from the projectile rear side in the sample (target) material superimpose resulting in tensile stresses in the sample. If the tensile stress exceeds the loading capacity of the material, the dynamic through thickness strength under uniaxial strain, or “spall strength” can be determined. Mode I delamination occurs and compressive release waves are generated, which limit the velocity decrease at the free target surface.

Figure 5-8 shows the experimental configuration. A cylindrical projectile is accelerated in a gas gun and normally impacts a stationary sample. A high resolution VISAR laser interferometer records the velocity increase on the target rear surface.

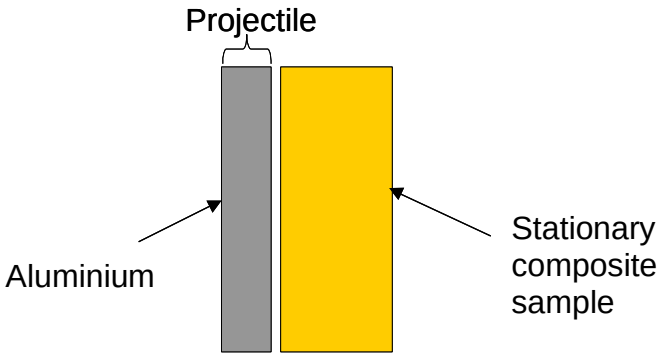

Figure 5-8 Experimental configuration of the direct plate impact experiment

The spall strength can then be calculated from the following equation,

$$\sigma_{sp} = \frac{1}{2}\rho_0 c_p \Delta u_{sp} \qquad (5\text{-}2)$$

where C_p is the soundspeed and ΔU_{sp} is the difference in velocity between the shocked state and the limit of spall strength signal.

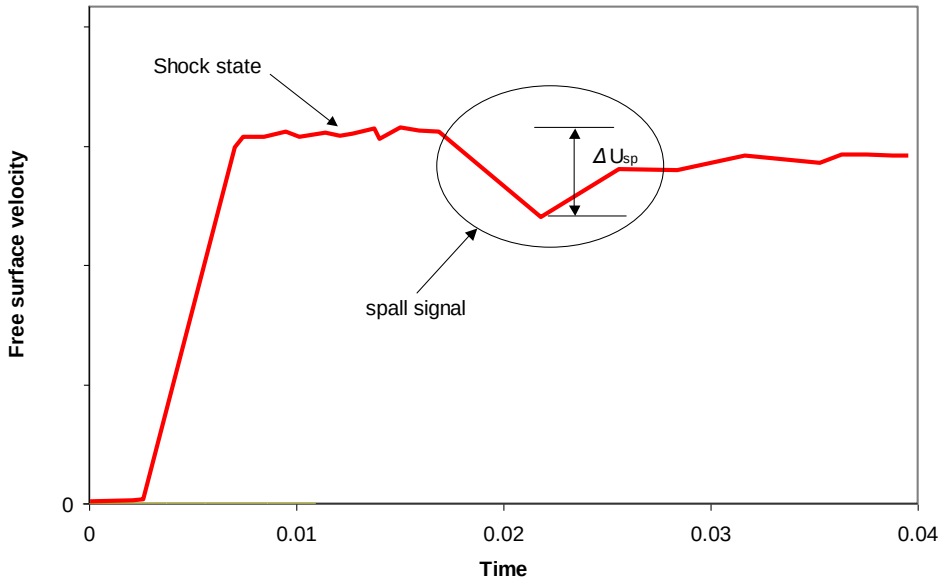

Figure 5-9 Typical velocity trace from a direct plate impact test

5.3.2 Double Cantilever Beam – Mode I Delamination Energy

The fracture energy for static mode I delamination can be measured using a 'Double Cantilever Beam', or DCB test [2]. The test sample has a crack placed into it during manufacture. This predefined crack is then extended by applying a load to the faces of the sample both above and below the crack. This can be achieved by gluing hinges onto each surface. These hinges are then clamped into experimental apparatus which pulls them apart. The test machine used to apply the load to the sample also allows the sample to move uniaxially along its length by a set of rollers as illustrated in Figure 5-10.

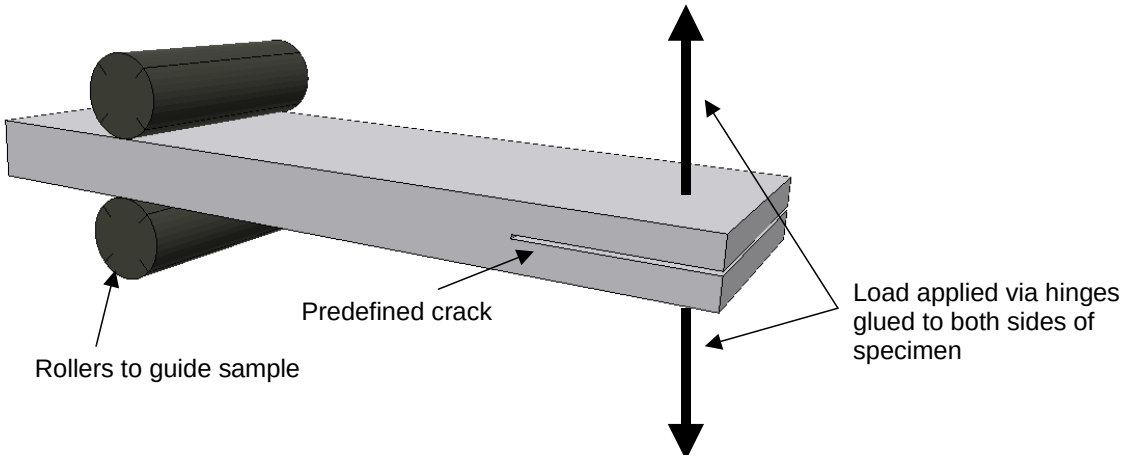

Figure 5-10 Illustration of the double cantilever beam test

The applied force and the displacement of the cantilevers are used to derive the energy consumed for crack propagation. The fracture energy G_{IC} is deduced by normalising over the delaminated area.

A typical force/displacement curve is displayed in Figure 5-11. Before the onset of crack propagation the slope of the curve is linear. Subsequently a decreasing force level is observed caused by an increasing lever of the test machine.

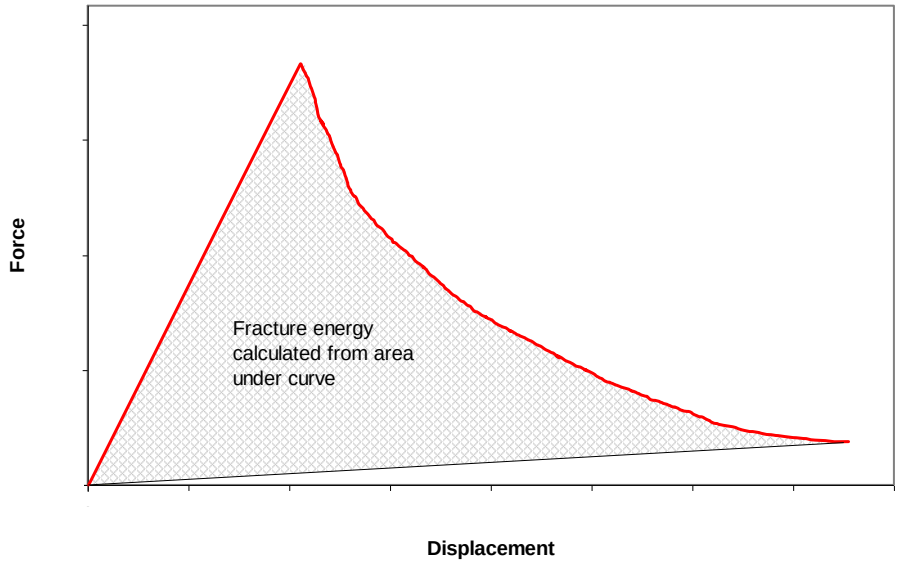

Figure 5-11 Force – displacement curve for determination of the Mode I fracture energy release rate

For full experimental details the reader should refer to [2].

5.3.3 Double Notch Shear – Mode II Delamination Strength

The interlaminar shear strength (ILSS), the stress st which Mode II delamination occurs, can be measured using a double notch shear test (DNS) This type of test should be performed according to standard proposal ASTM D 3846-79 [10].

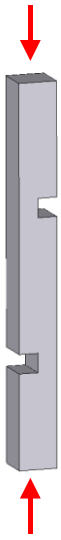

Figure 5-12 Configuration of short beam shear test sample

Figure 5-12 shows the geometry of a typical DNS specimen. Two notches are machined into the sample, one on either side, up to the same laminate layer. The sample is then axially compressed in a servo-hydraulic testing machine inducing shear loading on the bond area in between the two notches. Measurements of applied load and displacement are recorded.

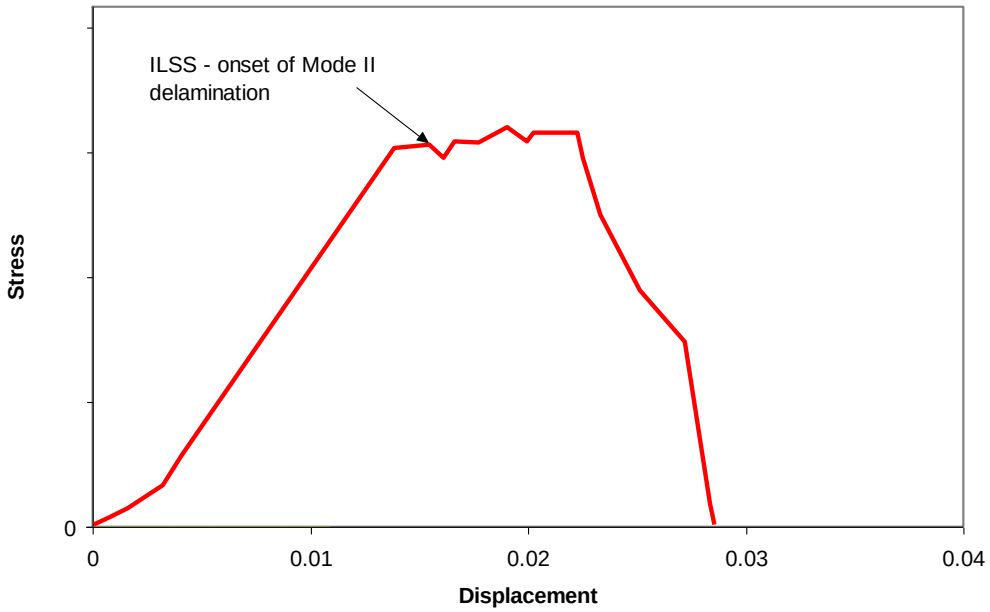

Figure 5-13 Typical output from DNS test: interlaminar shear strength

Figure 5-13 shows the typical output from a DNS experiment. The stress is calculated as the maximum load divided by the cross section between the two notches of the specimen. The interlaminar shear strength corresponds to the maximum stress at failure.

5.3.4 End Notched Flexure - Mode II Delamination Energy

In Mode II delamination failure occurs due to excessive shear stress. The end notched flexure (ENF) test determines the elastic energy threshold required for the growth of a predefined delamination for this mode of failure.

Such a test should be performed to the standard proposal EN 6034 [11]. Figure 5-14 shows a schematic of the experimental set-up and geometry of the sample. The sample, containing a predefined crack is loaded in a test machine in a three point bending configuration. Displacement of the loading device and applied load is recorded continuously during the tests.

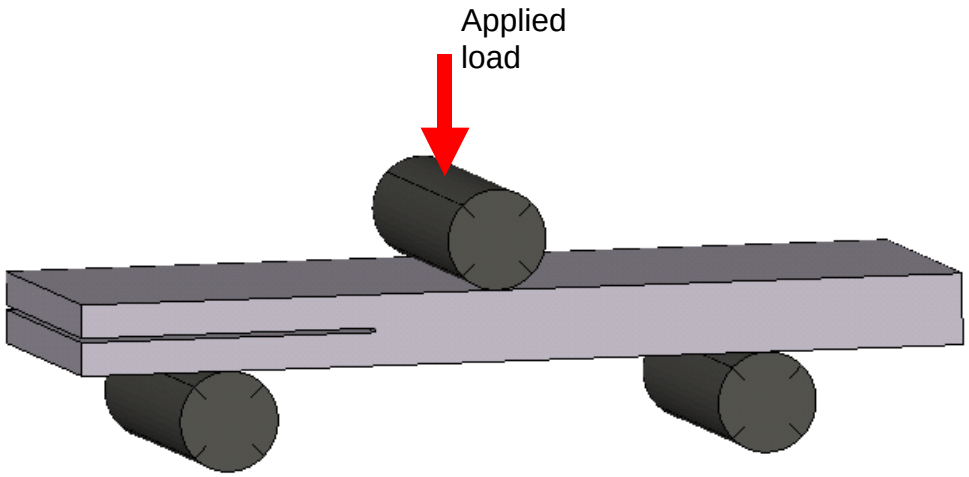

Figure 5-14 Schematic of theENF configuration used to determine the interlaminar fractur energy G_{IIC}

The predefined crack grows further as a result of the Mode II loading: specimen bending and the resultant shear forces at the crack tip. The total fracture toughness energy G_{IIc} is calculated from the initial crack length and from the critical load P to start the crack, and, the displacement of the test machine d at onset of crack extension [11]. All remaining coefficients are sample and test rig dimensions. Further detailed information can be found in [2].

$$G_{IIC} = \frac{9 \cdot P \cdot a^2 \cdot d \cdot 1000}{2 \cdot w\,(1/4l^3 + 3a^3)} \qquad (5\text{-}3)$$

The interlaminar fracture toughness energy is the energy per unit plate width that is necessary to grow an interlaminar crack. A typical force displacement curve is presented in Figure 5-15 and shows an interruption of the initial slope in the force displacement curve characterising the critical load at the onset of crack propagation in the specimen. Afterwards, the reduced bending stiffness influences the force displacement curve.

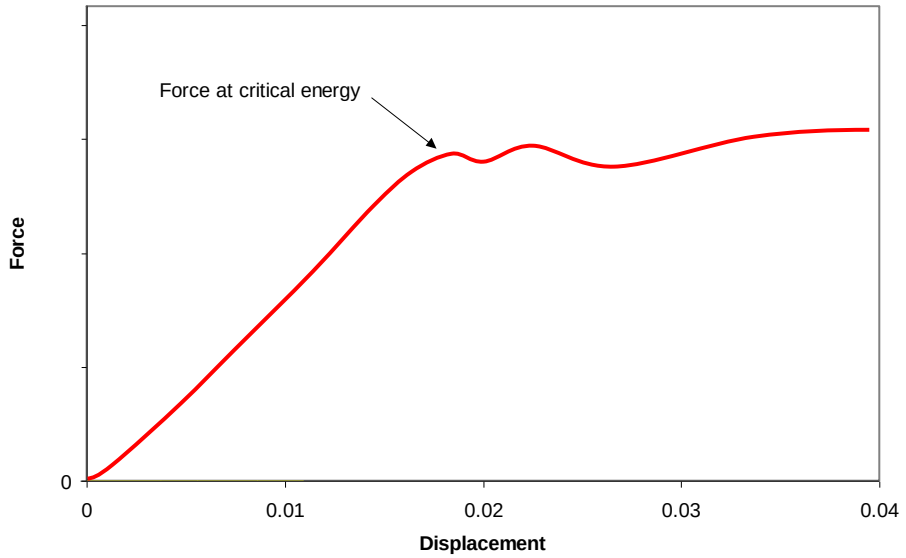

Figure 5-15 Typical load displacement curve for determination of the Mode II interlaminar fracture energy

6 Derivation of Material Properties

In this section of the document we discuss derivation of the material parameters required for the various orthotropic material modelling options from the experiments outlined in 5.

6.1 Constitutive Properties

6.1.1 Elastic Properties

The input data required for the orthotropic material model in AUTODYN can be entered in two ways. The user has the option to specify the elastic engineering constants directly by selecting “Engineering” for the input type, or the stiffness matrix coefficients may be input by choosing “Matrix Coefficients”. This option has been implemented since some stiffness matrix coefficients are obtained directly experimental tests. For example, depending on the application, C_{11} may be calculated directly from a uniaxial strain experiment such as the inverse flyer plate tests of 5.2.1.

The stiffness matrix coefficients, in terms of the elastic engineering constants, can be calculated from the following expressions obtained by inverting the compliance matrix (3-6),

$$
\begin{aligned}
C_{11} &= \frac{1-\nu_{23}\nu_{32}}{E_{22}E_{33}\Delta} \\
C_{12} &= \frac{\nu_{21}+\nu_{31}\nu_{23}}{E_{22}E_{33}\Delta} = \frac{\nu_{12}+\nu_{32}\nu_{13}}{E_{11}E_{33}\Delta} \\
C_{13} &= \frac{\nu_{31}+\nu_{21}\nu_{32}}{E_{22}E_{33}\Delta} = \frac{\nu_{13}+\nu_{12}\nu_{23}}{E_{11}E_{22}\Delta} \\
C_{22} &= \frac{1-\nu_{13}\nu_{31}}{E_{11}E_{33}\Delta} \\
C_{23} &= \frac{\nu_{32}+\nu_{12}\nu_{31}}{E_{11}E_{33}\Delta} = \frac{\nu_{23}+\nu_{21}\nu_{13}}{E_{11}E_{22}\Delta} \\
C_{33} &= \frac{1-\nu_{12}\nu_{21}}{E_{11}E_{22}\Delta} \\
C_{44} &= 2G_{23} \\
C_{55} &= 2G_{31} \\
C_{66} &= 2G_{12}
\end{aligned}
\qquad (6\text{-}1)
$$

where

$$
\Delta = \frac{1-\nu_{12}\nu_{21}-\nu_{23}\nu_{32}-\nu_{31}\nu_{13}-2\nu_{21}\nu_{32}\nu_{13}}{E_{11}E_{22}E_{33}}.
$$

Table 6-1 outlines the experimental tests used to calculate values for the engineering elastic constants.

Property	Description

E_{11}	Through thickness Youngs Modulus Not measured directly. Can be calculated from $\frac{\nu_{12}}{E_{11}} = \frac{\nu_{21}}{E_{22}}$ to ensure a consistent stiffness matrix, or can be estimated from inverse flyer plate tests, see Section 6.2
E_{22}	In-plane Youngs Modulus. Calculated from 0° tension tests
E_{33}	In-plane Youngs Modulus. Calculated from 90° tension tests
ν_{23}	In-plane Poissons ratio. Calculated from 0° tension tests in which strain gauges applied in 22 & 33 directions
ν_{31}	Out-of-plane Poissons ratio. Calculated from 90° tension tests in which strain gauges applied in 11 & 33 directions
ν_{12}	Out-of-plane Poissons ratio Often unknown, can be calculated from $\frac{\nu_{12}}{E_{11}} = \frac{\nu_{21}}{E_{22}}$ if ν_{21} calculated from 0° tension tests in which strain gauges applied in 11 & 22 directions and E_{11} known or estimated.
G_{23}	In-plane shear modulus Average of that calculated from 45° tensile tests using (6-2) below.
G_{12}	Out-of-plane shear modulus Average value calculated from short beam shear tests
G_{31}	Out-of-plane shear modulus As G_{12} above

Table 6-1 Derivation of orthotropic material elastic properties

The in-plane shear modulus G_{23} is calculated from the following equation [7] where E_y is the modulus measured in 45° tension test described in 5.1.1.2,

$$G_{23} = \frac{1}{\left(\frac{4}{E_Y} - \frac{1}{E_{22}} - \frac{1}{E_{33}} + \frac{2\nu_{23}}{E_{22}}\right)} \tag{6-2}$$

6.1.2 Plasticity Parameters

As with an isotropic yield criteria that includes work hardening, we can use a uniaxial tension test to obtain the relationship between $\bar{\sigma}$ and $d\bar{\varepsilon}^P$. In practice the master $\bar{\sigma} - \bar{\varepsilon}^p$ curve can be calculated from any normal or shear stress-strain test. In this example we choose to use a 0° uniaxial tension test.

In this case the quadratic yield function (3-29) reduces to,

$$f(\sigma_{ij}) = a_{22}\sigma_{22}^2 \tag{6-3}$$

and using the definition of effective stress (3-38), the relationship between effective stress and σ_{22} is

$$\bar{\sigma} = \sqrt{\frac{3}{2} a_{22} \sigma_{22}} \tag{6-4}$$

Actually, in general for uniaxial loading the following relationship results

$$\bar{\sigma} = \sqrt{\frac{3}{2} a_{ii} \sigma_{ii}} \quad \text{, no summation on repeated indices} \tag{6-5}$$

and, from (3-33) the associated incremental plastic strain components are

$$d\varepsilon_{jj}^{P} = \frac{a_{ji}}{a_{ii}} d\varepsilon_{jj}^{P} \,, \quad d\varepsilon_{kk}^{P} = \frac{a_{ik}}{a_{ii}} d\varepsilon_{kk}^{P} \,, \quad d\varepsilon_{ij}^{P} = 0 \qquad (i \neq j) \tag{6-6}$$

On substitution of (6-6) into the expression for incremental effective plastic strain (3-40) we find that for uniaxial loadings

$$d\bar{\varepsilon}^{P} = \sqrt{\frac{2}{3a_{ii}}} d\varepsilon_{ii}^{P} \quad \text{, no summation over repeated indices} \tag{6-7}$$

For pure shear loading the same arguments result in the following relationship for effective stress and effective plastic strain increment,

$$\bar{\sigma} = \sqrt{3a_{rr}}\, \sigma_{ij} \tag{6-8}$$

$$d\bar{\varepsilon}^{P} = 2 d\varepsilon_{ij}^{P} \Big/ \sqrt{3a_{rr}} \tag{6-9}$$

where rr=44,55 or 66 depending on shear stress components.

Derivation of the plasticity parameters is best illustrated by an example. In the following discussion results from tension tests on a 0°/90° woven Kevlar-epoxy composite material are presented [2]. In this case the stress-strain behaviour in the 0°, or 22 direction, is considered to define the master $\bar{\sigma} - \bar{\varepsilon}^{p}$ curve. The plasticity parameter a_{22} in this case is a free parameter and we are at liberty to set its value simply to 1.0. Equations (6-5) and (6-6) are now used to transform the measured values of σ_{22} and ε_{22} into effective stresses and effective incremental plastic strains thus determining the required master curve, as shown in Figure 6-1.

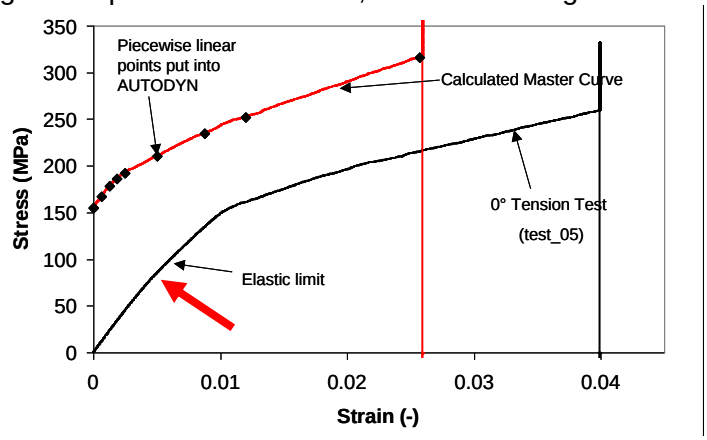

Figure 6-1 Derivation of master $\bar{\sigma} - \bar{\varepsilon}^{p}$ relationship from uniaxial tension test

Kevlar-epoxy is a 0°/90° woven material and is assumed to be transversely isotropic, therefore $a_{22}=a_{33}=1.0$. The in-plane plastic Poisson's ratio ν_{23}^{P} was calculated as 0.26 from 0° tension tests where strain was measured in both in-plane directions. It was calculated from the average gradient of measured strains immediately after yielding, see Figure 6-2 below.

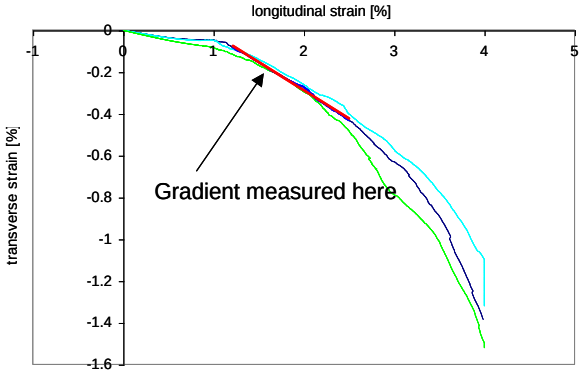

Figure 6-2 Longitudinal versus transverse strain measured in 0° tension tests. Red line indicates region used to calculate value for in-plane Poissons ratio. (Picture courtesy of EMI [2])

Therefore from (3-35) a_{23} can now be calculated as follows:

$$\begin{aligned} a_{23} &= -a_{22}\nu_{23}^{P} \\ &= -1.0 \times 0.26 \\ &= -0.26 \end{aligned} \tag{6-10}$$

The out-of-plane PPR ν_{21}^{P} was estimated as 0.698 from the 0° tension tests where strain was additionally measured in the through thickness direction.

Therefore from (3-35) a_{12}, and hence a_{13}, can now be calculated as follows:

$$\begin{aligned} a_{12} &= -a_{22}\nu_{21}^{P} \\ &= -1 \times 0.698 \\ &= 0.698 \end{aligned} \tag{6-11}$$

$$\begin{aligned} a_{13} &= -a_{33}\nu_{31}^{P} \\ &= -1 \times 0.698 \\ &= 0.698 \end{aligned} \tag{6-12}$$

The a_{44} plasticity coefficient was calibrated through simulation of the uniaxial tension test with loading at +/- 45° to the fibres. Using the plasticity coefficients derived so far in this section the quadratic yield function is sufficiently described to allow a_{44} to be modified until the 45° tension test results were reproduced.

Best agreement with experiment is achieved with $a_{44} = 4.0$, see Figure 6-3.

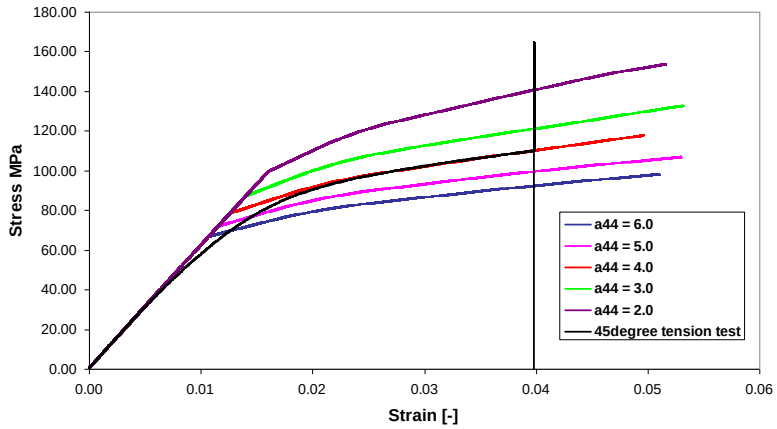

Figure 6-3 Results from simulations of 45° tension tests. (Experimental result courtesy of EMI [2])

In the absence of further experimental data it was assumed the out-of-plane shear plasticity coefficients are equal to the in-plane properties. Therefore,

$$a_{55} = a_{66} = 4.0 \qquad (6\text{-}13)$$

6.2 Equation of State Parameters

Figure 6-4 compares the results of simulations of inverse flyer plate tests on a Kevlar-epoxy composite material to experiment. The blue velocity trace is recorded in a simulation that used an orthotropic model with a linear equation of state. It is obvious that the initial Hugoniot states are under predicted. However a much improved correspondence with experiment is achieved when using the orthotropic material model a polynomial equation of state.

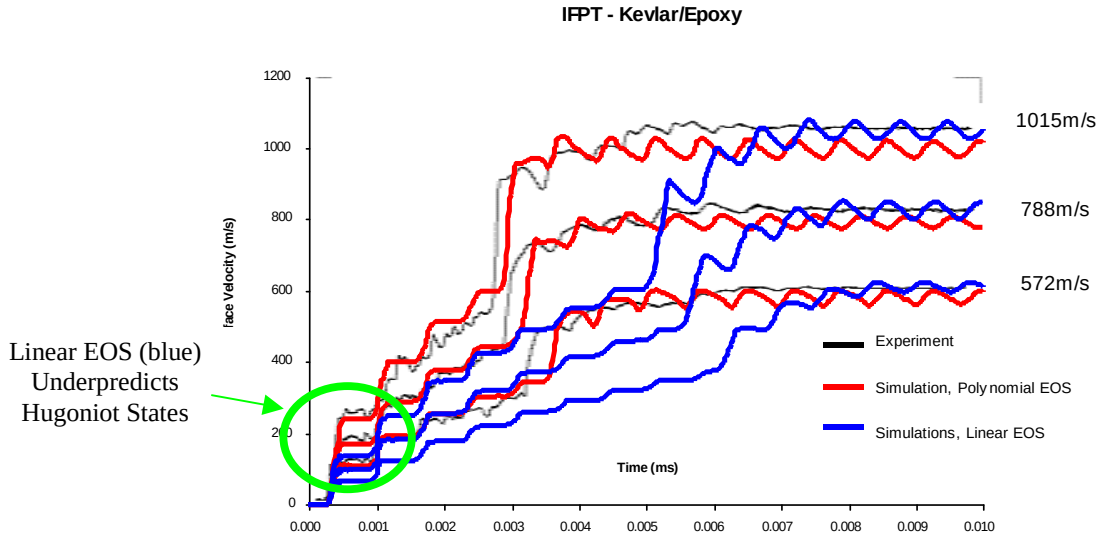

Figure 6-4 Kevlar/Epoxy IFPT, Influence of Shock Effects. (Experimental result courtesy of EMI [1])

Based on the results of Figure 6-4 a plot of the derived Hugoniot impact states is given in terms of shock- versus particle-velocity points in Figure 6-5. Further details

of this can be found in [1][2]. Kevlar-epoxy exhibits typical solid behaviour with shock velocity approximately increasing linearly with particle velocity.

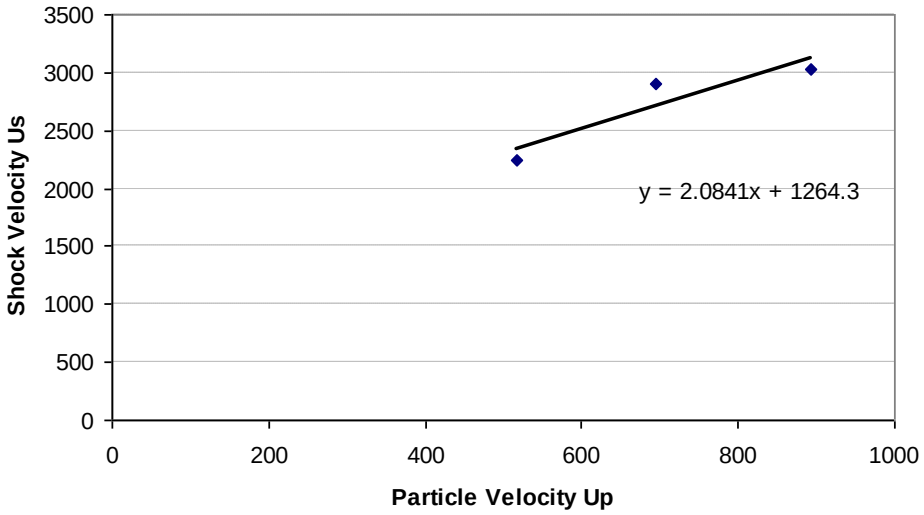

Figure 6-5 Shock velocity versus particle velocity relationship for Kevlar-epoxy inverse flyer plate tests. (Data courtesy of EMI [1])

If the application being modelled requires use of a non-linear equation of state in conjunction with an orthotropic material model then the gradient and intercept of the line in Figure 6-5 can be directly input as the S1 and C1 inputs, respectively, for a shock equation of state.

Alternatively, a polynomial equation of state may be used. In this case the A1 term is calculated as the effective bulk modulus. The A2 and A3 terms may then be calibrated by simulation to give best agreement with experiment. This is indeed the approach used to obtain the results of Figure 6-4.

Assuming that the 11-direction is defined as being through the thickness of the composite material it is possible to calculate the C_{11} stiffness matrix coefficient. Since the flyer plate tests are approximately uniaxial in strain the following expression applies,

$$C_{11} = \rho C_B^2 . \qquad (6\text{-}14)$$

6.3 Failure/Softening Properties

6.3.1 Failure Properties

The failure initiation stresses can be derived from experiment as described in Table 6-2.

Property	Experimental Test
σ_{11fail}	Calibrated to experiment to give good agreement with spall plate tests and DCB
σ_{22fail}	0° or 90° tension test depending on orientation of material directions
σ_{33fail}	0° or 90° tension test depending on orientation of material directions

σ_{31fail}	Interlaminar shear strength test
σ_{23fail}	45° tension test and calibration via simulation
σ_{12fail}	Interlaminar shear strength test

Table 6-2 Failure properties and the tests they are measured from

6.3.2 Softening Properties

The fracture energies utilised to control the rate of crack growth in each cell are obtained from the experiments detailed in 5.3 as described below in Table 6-3.

Property	Experimental Test
Mode I delamination 11 - Gf_{11}	DCB test
Gf_{22}	Calibrate simulation to 0° tension test
Gf_{33}	Calibrate simulation to 0° tension test
Mode II delamination 13 – Gf_{13}	ENF test
Gf_{12} (same as 13 direction)	ENF test
Gf_{23}	Assumed to be same as other shear directions

Table 6-3 Fracture energies and tests from which they may be derived

6.4 Calculating Laminate Properties from Uni-Directional Data

Laminates made from composite materials often consist of a number of repeating sublaminates or individual lamina. Typically material data may be available for a uni-directional lamina and it is therefore desirable to be able to be able to calculate the effective material properties for the laminate from the constituent lamina properties.

This is also useful since within AUTODYN each layer of the laminate is not explicitly modelled, rather continuum elements representing equivalent homogeneous anisotropic solids are used to represent thick laminates consisting of a number of repeating lamina.

The approach of Sun and Li [4] has successfully been used to calculate laminate properties for use in AUTODYN and is now described.

Consider a laminate consisting of *N* orthotropic fibre composite lamina of arbitrary fibre orientations. In the following description the *x* and *y* co-ordinates are in the plane of the composite and *z* is through the thickness. The effective macro-stress and macro-strains are defined to give,

$$\overline{\sigma}_{ij} = \sum_{k=1}^{N} v_k \, \sigma_{ij}^{(k)} \qquad (6\text{-}15)$$

$$\overline{\varepsilon}_{ij} = \sum_{k=1}^{N} v_k \, \varepsilon_{ij}^{(k)} \qquad (6\text{-}16)$$

where $\sigma_{ij}^{(k)}$ and $\varepsilon_{ij}^{(k)}$ are the stresses and strains in the k^{th} lamina and, if t_k is the lamina thickness and *h* the total thickness

$$v_k = \frac{t_k}{h} = \text{volume fraction of the k}^{\text{th}} \text{ lamina} \tag{6-17}$$

The effective elastic properties for the laminate are given by,

$$\begin{pmatrix} \overline{\sigma}_{xx} \\ \overline{\sigma}_{yy} \\ \overline{\sigma}_{zz} \\ \overline{\sigma}_{yz} \\ \overline{\sigma}_{xz} \\ \overline{\sigma}_{xy} \end{pmatrix} = \left[\overline{C}\right] \begin{pmatrix} \overline{\varepsilon}_{xx} \\ \overline{\varepsilon}_{yy} \\ \overline{\varepsilon}_{zz} \\ \overline{\gamma}_{yz} \\ \overline{\gamma}_{xz} \\ \overline{\gamma}_{xy} \end{pmatrix} \tag{6-18}$$

The x-y plane for a lamina is a plane of symmetry and is also a symmetry plane for the effective solid. Therefore the effective stiffness matrix reduces to the following form,

$$\left[\overline{C}\right] = \begin{bmatrix} \overline{c}_{11} & \overline{c}_{12} & \overline{c}_{13} & 0 & 0 & \overline{c}_{16} \\ \overline{c}_{12} & \overline{c}_{22} & \overline{c}_{23} & 0 & 0 & \overline{c}_{26} \\ \overline{c}_{13} & \overline{c}_{23} & \overline{c}_{33} & 0 & 0 & \overline{c}_{36} \\ 0 & 0 & 0 & \overline{c}_{44} & \overline{c}_{45} & 0 \\ 0 & 0 & 0 & \overline{c}_{45} & \overline{c}_{55} & 0 \\ \overline{c}_{16} & \overline{c}_{26} & \overline{c}_{36} & 0 & 0 & \overline{c}_{66} \end{bmatrix} \tag{6-19}$$

and effective compliance matrix is calculated as,

$$\left[\overline{S}\right] = \left[\overline{C}\right]^{-1} \tag{6-20}$$

where the effective elastic properties are then,

$$\begin{aligned} \overline{E}_{xx} &= \frac{1}{\overline{S}_{11}} \qquad \overline{E}_{yy} = \frac{1}{\overline{S}_{22}} \qquad \overline{E}_{zz} = \frac{1}{\overline{S}_{33}} \\ \overline{\nu}_{yz} &= -\frac{\overline{S}_{23}}{\overline{S}_{22}} \qquad \overline{\nu}_{xz} = -\frac{\overline{S}_{31}}{\overline{S}_{11}} \qquad \overline{\nu}_{xy} = -\frac{\overline{S}_{21}}{\overline{S}_{11}} \\ \overline{G}_{yz} &= \frac{1}{\overline{S}_{44}} \qquad \overline{G}_{xz} = \frac{1}{\overline{S}_{55}} \qquad \overline{G}_{xy} = \frac{1}{\overline{S}_{66}} \end{aligned} \tag{6-21}$$

After lengthy algebraic manipulations the following expressions are recovered for the effective stiffness matrix coefficients [4],

$$\bar{c}_{11} = \sum_{k=1}^{N} v_k c_{11}^{(k)} + \sum_{k=2}^{N} \left(c_{13}^{(k)} - \bar{c}_{13}\right) v_k \left(c_{13}^{(1)} - c_{13}^{(k)}\right) \Big/ c_{33}^{(k)}$$

$$\bar{c}_{12} = \sum_{k=1}^{N} v_k c_{12}^{(k)} + \sum_{k=2}^{N} \left(c_{13}^{(k)} - \bar{c}_{13}\right) v_k \left(c_{23}^{(1)} - c_{23}^{(k)}\right) \Big/ c_{33}^{(k)}$$

$$\bar{c}_{13} = \sum_{k=1}^{N} v_k c_{13}^{(k)} + \sum_{k=2}^{N} \left(c_{33}^{(k)} - \bar{c}_{33}\right) v_k \left(c_{13}^{(1)} - c_{13}^{(k)}\right) \Big/ c_{33}^{(k)}$$

$$\bar{c}_{22} = \sum_{k=1}^{N} v_k c_{22}^{(k)} + \sum_{k=2}^{N} \left(c_{23}^{(k)} - \bar{c}_{23}\right) v_k \left(c_{23}^{(1)} - c_{23}^{(k)}\right) \Big/ c_{33}^{(k)}$$

$$\bar{c}_{23} = \sum_{k=1}^{N} v_k c_{23}^{(k)} + \sum_{k=2}^{N} \left(c_{33}^{(k)} - \bar{c}_{33}\right) v_k \left(c_{23}^{(1)} - c_{23}^{(k)}\right) \Big/ c_{33}^{(k)}$$

$$\bar{c}_{33} = 1 \Big/ \left(\sum_{k=1}^{N} v_k \, / \, c_{33}^{(k)} \right) \qquad \text{(6-22)}$$

$$\bar{c}_{16} = \sum_{k=1}^{N} v_k c_{16}^{(k)} + \sum_{k=2}^{N} \left(c_{13}^{(k)} - \bar{c}_{13}\right) v_k \left(c_{36}^{(1)} - c_{36}^{(k)}\right) \Big/ c_{33}^{(k)}$$

$$\bar{c}_{26} = \sum_{k=1}^{N} v_k c_{26}^{(k)} + \sum_{k=2}^{N} \left(c_{23}^{(k)} - \bar{c}_{23}\right) v_k \left(c_{36}^{(1)} - c_{36}^{(k)}\right) \Big/ c_{33}^{(k)}$$

$$\bar{c}_{36} = \sum_{k=1}^{N} v_k c_{36}^{(k)} + \sum_{k=2}^{N} \left(c_{33}^{(k)} - \bar{c}_{33}\right) v_k \left(c_{36}^{(1)} - c_{36}^{(k)}\right) \Big/ c_{33}^{(k)}$$

$$\bar{c}_{66} = \sum_{k=1}^{N} v_k c_{66}^{(k)} + \sum_{k=2}^{N} \left(c_{36}^{(k)} - \bar{c}_{36}\right) v_k \left(c_{36}^{(1)} - c_{36}^{(k)}\right) \Big/ c_{33}^{(k)}$$

$$\bar{c}_{44} = \left(\sum_{k=1}^{N} v_k c_{44}^{(k)} \Big/ \Delta_k \right) \Big/ \Delta$$

$$\bar{c}_{45} = \left(\sum_{k=1}^{N} v_k c_{45}^{(k)} \Big/ \Delta_k \right) \Big/ \Delta$$

$$\bar{c}_{55} = \left(\sum_{k=1}^{N} v_k c_{55}^{(k)} \Big/ \Delta_k \right) \Big/ \Delta$$

where,

$$\Delta = \left(\sum_{k=1}^{N} v_k c_{44}^{(k)} \Big/ \Delta_k \right) \left(\sum_{k=1}^{N} v_k c_{55}^{(k)} \Big/ \Delta_k \right) - \left(\sum_{k=1}^{N} v_k c_{45}^{(k)} \Big/ \Delta_k \right)^2$$

$$\Delta_k = c_{44}^{(k)} c_{55}^{(k)} - \left(c_{45}^{(k)}\right)^2$$

The principal material directions of all the lamina in the laminate will not necessarily be aligned with the global axes. Therefore, before the above summations can be performed it will be necessary to transform the stiffness matrix for each lamina as follows,

$$\left[C^{(k)}\right] = \left[T^{(k)}\right]^{-1} \left[C^{(k)}\right] \left[T^{(k)}\right]^{-T} \qquad \text{(6-23)}$$

where the transformation matrix *T* is defined as,

$$\left[T^{(k)}\right]=\begin{bmatrix} \cos^2\theta & \sin^2\theta & 0 & 0 & 0 & \sin 2\theta \\ \sin^2\theta & \cos^2\theta & 0 & 0 & 0 & -\sin 2\theta \\ 0 & 0 & 1 & 0 & 0 & 0 \\ 0 & 0 & 0 & \cos\theta & -\sin\theta & 0 \\ 0 & 0 & 0 & \sin\theta & \cos\theta & 0 \\ -\sin 2\theta/2 & \sin 2\theta/2 & 0 & 0 & 0 & \cos 2\theta \end{bmatrix} \quad (6\text{-}24)$$

and the angle θ is the angle of the material directions with regards to the global axes.

7 Example Applications

The composite material models available in AUTODYN and described throughout this report have been validated through application to a wide variety of loading conditions. In this section of the report a selection of these applications are presented.

7.1 Hypervelocity Impacts

7.1.1 Advanced Material Model for Hypervelocity Impact Simulations

This summary describes the work carried out by the Ernst-Mach-Institute (EMI), Century Dynamics Ltd (CDL) and TNO Prins Maurits Laboratorium (TNO) under ESA research contract No. 12400/97/NL/PA(SC) [1]. The aim of this project, termed AMMHIS, was to develop and define advanced material models and data for Nextel and Kevlar/Epoxy under hypervelocity impact conditions. The AMMHIS project was particularly concerned with the materials for the spacecraft shielding configuration used to protect the European Columbus module of the ISS. Due to the experimentally observed behaviour of Nextel and Kevlar-epoxy, a new orthotropic hydrocode model was developed. This was necessary because pressure inside these materials depends on deviatoric strain components as well as volumetric strain. Non-linear effects, such as shock effects, can be incorporated through the volumetric straining in the material. The developed model includes orthotropic material stiffness and a non-linear equation of state and is described in 3.2 of this report.

The hypervelocity impact of aluminium projectiles up to 15mm in diameter and normal velocities in the range of 3 km/s to 15 km/s were considered. The quality of the model has been demonstrated by comparison of simulations with tests to characterise the involved materials as well as with impact tests on the complete shielding configuration.

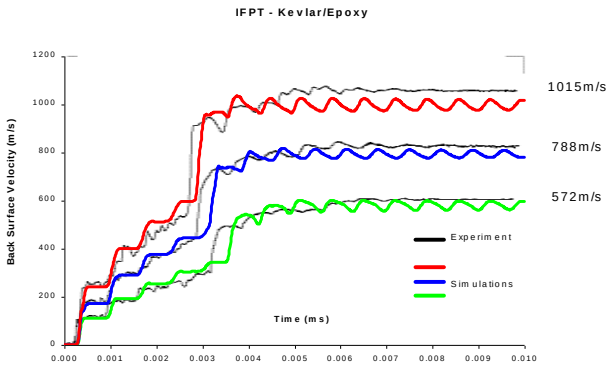

Back Surface Velocities, Experiment and Simulations

Figure 7-1 Inverse Flyer Plate Tests, Experimental and AMMHIS Model Results

The developed material model is able to predict the main aspects of the shielding material response. Calculated shielding damage in the first bumper and in the Nextel and Kevlar-epoxy layers correlates well with experimental results. In terms of the back wall damage; for the 3km/s impact the simulation predicts a small hole that was

not observed in the experiment, for the 6km/s impact the predicted back wall damage is consistent with the experimental observations (Figure 7-2 and Figure 7-3). The simulation sensitivity studies carried out at both these velocities suggest that these are marginal cases in terms of back wall penetration.

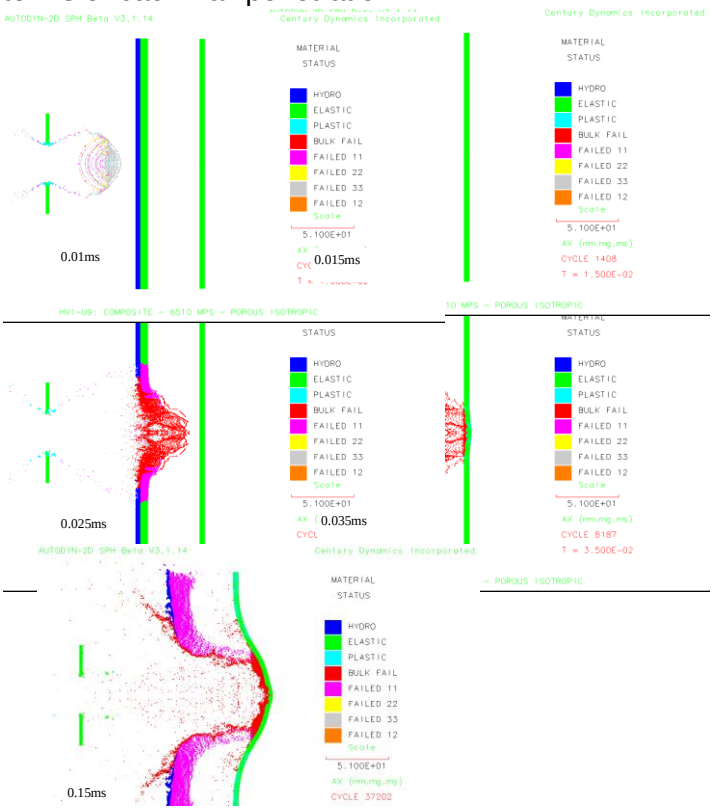

AUTODYN-2D SPH Simulation, AMMHIS Model
Material Status

Figure 7-2 Alenia/EMI Test A8611 on Reference Shielding, 15mm Diameter Projectile, 6.5km/s.

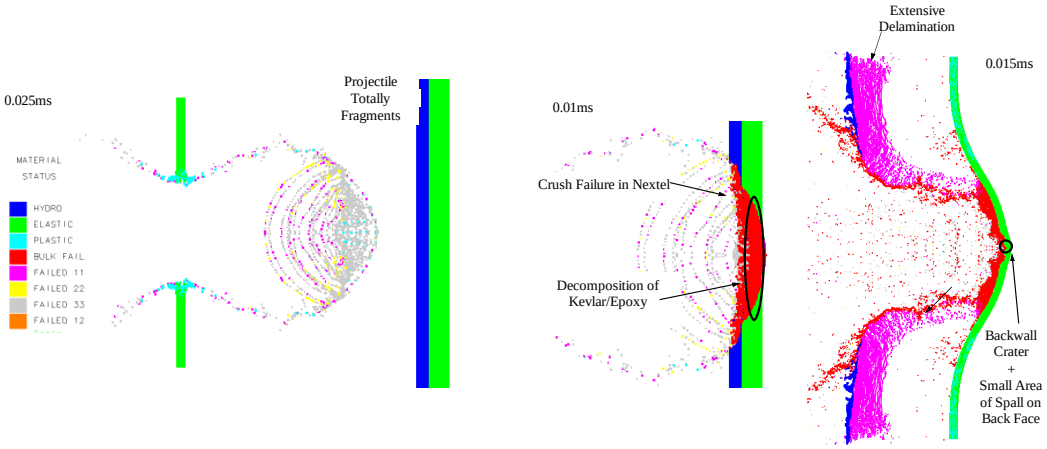

AUTODYN-2D SPH Simulation, Key Features of Material Response During Impact

Figure 7-3 Alenia/EMI Test A8611 on Reference Shielding, 15mm Diameter Projectile, 6.5km/s

7.1.2 Advanced Material Damage Models

This summary describes the work carried out by the Ernst-Mach-Institute (EMI) and Century Dynamics Ltd (CDL) under ESA research contract No. 12400/97/NL/PA(SC), CCN No. 2 [2]. The aim of this project, termed ADAMMO, was to develop and further improve the composite material characterisation and modelling techniques for modelling hypervelocity impact conditions based on the study of Section 7.1.1. The focus of the study was to allow better prediction of the levels of damage and residual strength in composite materials after impact. A methodology was implemented to incorporate anisotropic hardening observed in some highly non-linear composite materials such as Kevlar-epoxy, whilst retaining the ability to couple the constitutive response to a non-linear equation of state. Simulations of static tensile tests agreed well with experiment, see Figure 7-4.

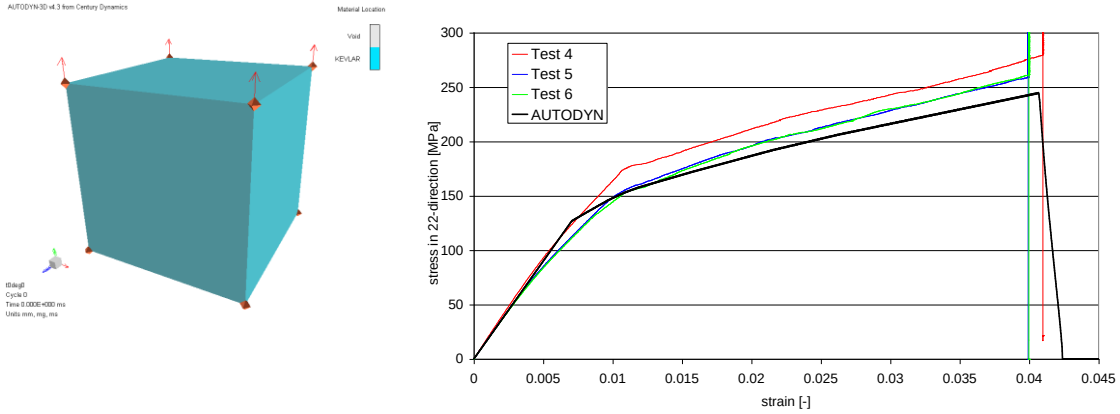

Figure 7-4 Results from simulation of 0° tension test

An orthotropic damage model, outlined in 4.2, was implemented into AUTODYN during the ADAMMO project. In short the softening behaviour observed in some composite materials is modelled using a crack softening approach where damage is accumulated as a function of crack strain and the ability of a laminate to carry tensile loads is reduced.

A simulation was performed with similar loading to that experienced by the material in a short beam bending test.

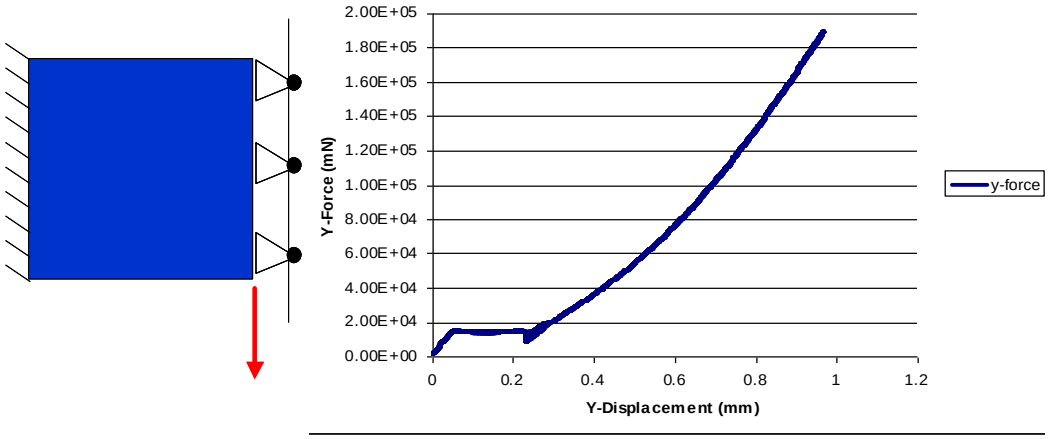

Figure 7-5 Simulation of short beam shear test

The resulting shear stress-deflection curve obtained from the simulation is shown in Figure 7-5. The response is linear elastic until the material begins to fail in shear after which a much reduced stiffness is initially observed. As the shear strain in the material continues to increase, the response hardens as the fibres re-orientate and

start to pick up the shear load. This behaviour is the same as that observed in the short beam bending characterisation test and demonstrates the versatility of the orthotropic model.

A number of the plate impact damage tests were simulated. In this test a symmetric assembly of Kevlar-epoxy and Al plates are used to prevent delamination caused by superposition of release waves. A schematic diagram of the test geometry is shown in Figure 7-6.

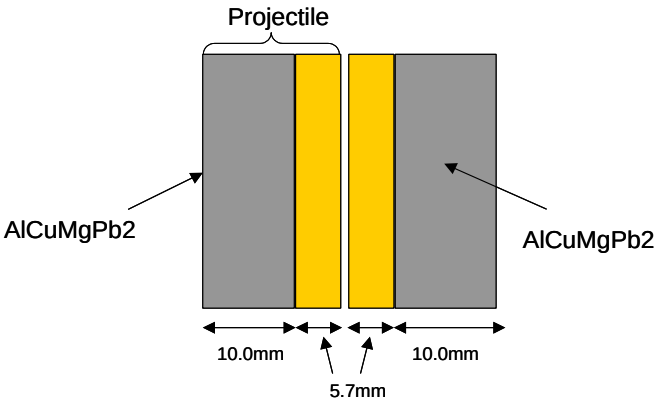

Figure 7-6 Schematic diagram of experimental set-up

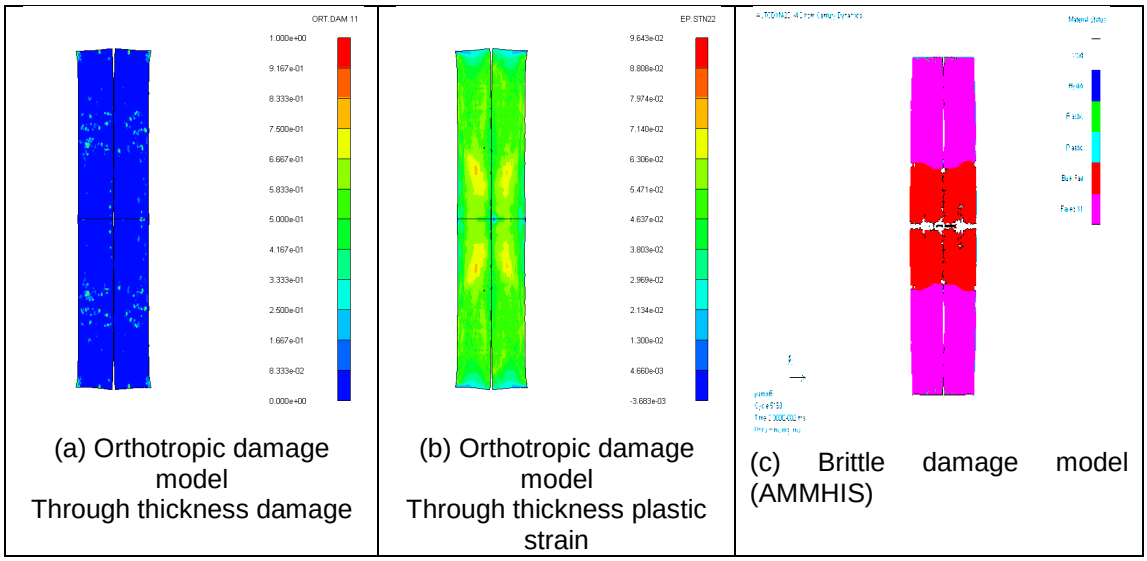

(a) Orthotropic damage model
Through thickness damage

(b) Orthotropic damage model
Through thickness plastic strain

(c) Brittle damage model (AMMHIS)

Figure 7-7 Simulation results of 276 m/s impact velocity

The orthotropic damage model predicts some damage for a 276m/s velocity impact, due to hardening of the material, Figure 7-7. This is close to the experimental result that shows limited amounts of delamination. The brittle damage model shows extensive delamination and even some bulk failure of the material which is clearly an over prediction of the levels of damage.

In conjunction with the hardening model described above, these additional orthotropic material models have been extensively validated by comparison with hypervelocity impact experiments. A series of debris cloud damage experiments were performed at EMI designed to generate impacted targets with damage gradients that are fully damaged in the central impact region and little damage at the extent of the targets.

Figure 7-8 show the simulation of test 4355 - a 8.2mm Al sphere impacting an 2.0mm Al bumper at 4.68km/s. The resulting debris cloud then impacts a 5.7mm thick Kevlar-epoxy target.

Figure 7-9 shows the final state of the simulation and the same configuration simulated without hardening included and using the brittle damage model (AMMHIS). The ADAMMO simulation produces much more compact level of damage with significant amounts of intact material remaining adjacent to the main impact zone as observed in experiment.

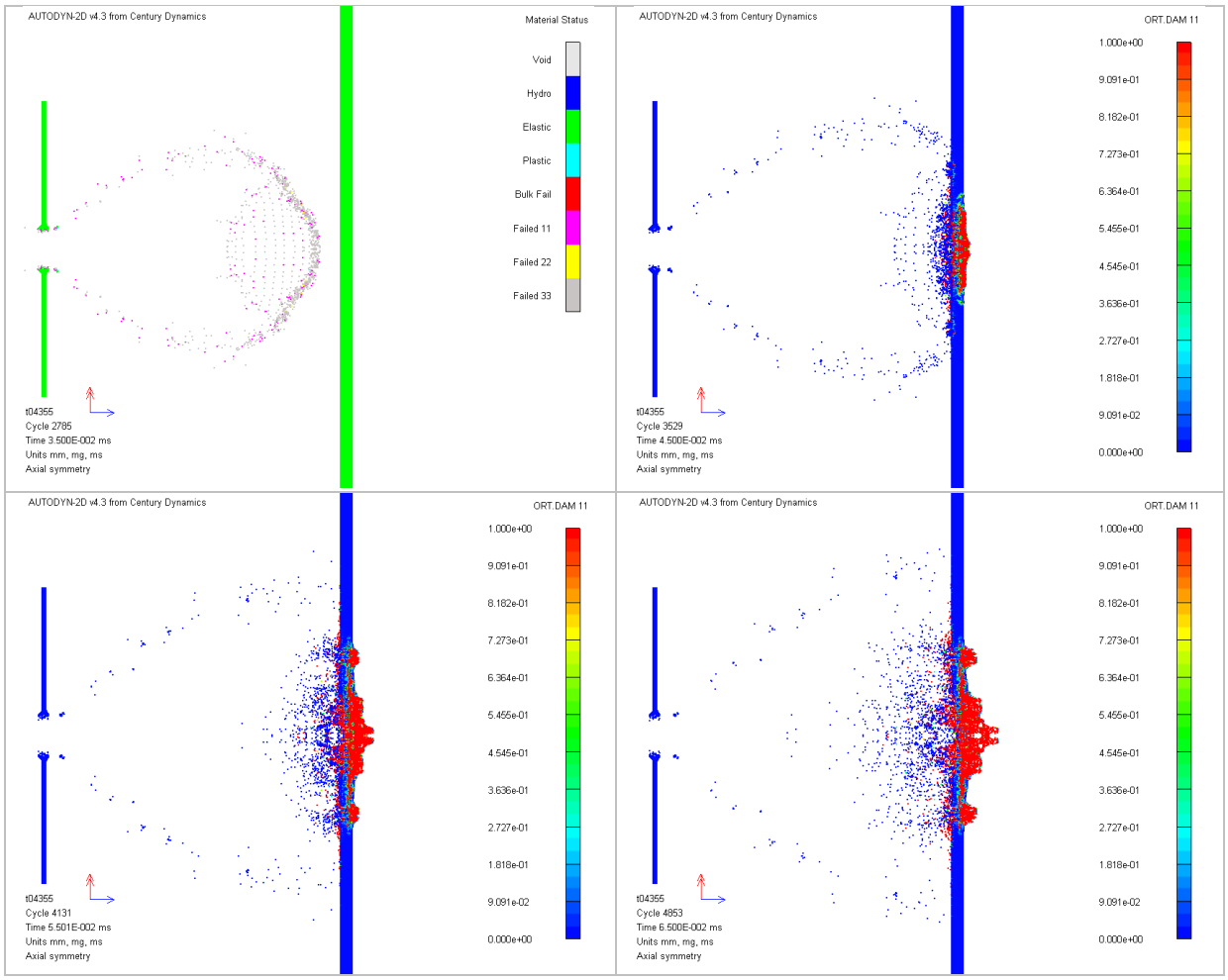

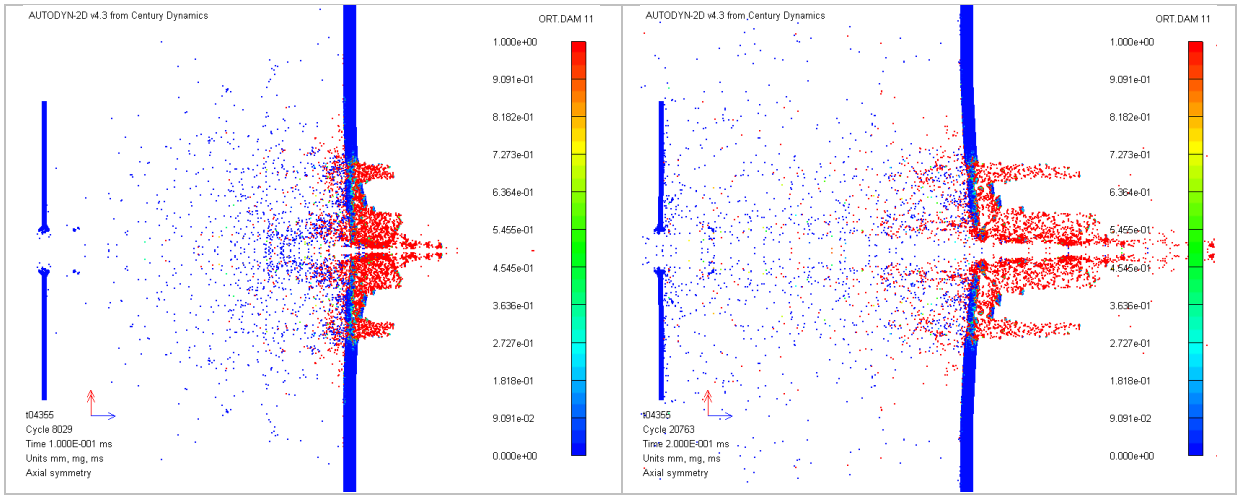

Figure 7-8 Test 4355 – through thickness damage during impact

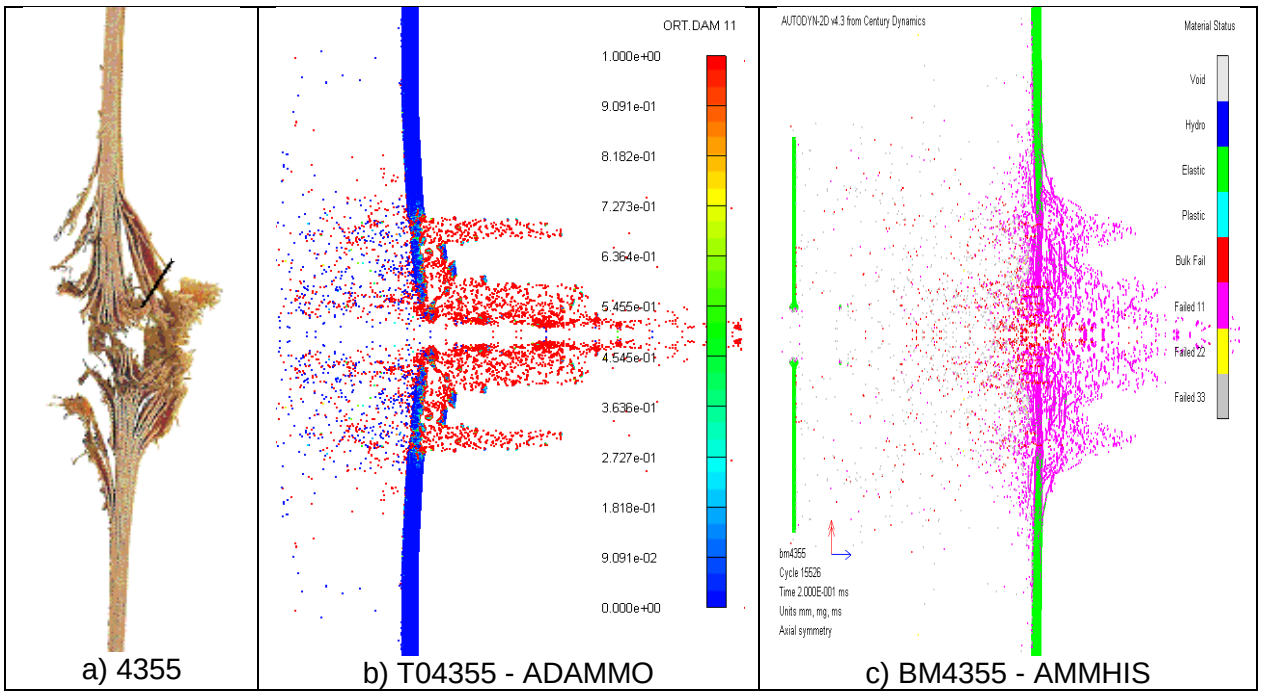

Figure 7-9 Final damage of test 4355

7.2 Ballistic Impact Examples

Composite and textile armour systems are increasingly being utilised as impact protection materials in weight critical environments. Applications range from protective shielding for space vehicles against hypervelocity impacts, to personal protective equipment of the soldier against ballistic threat. The use of composite and textile armour systems can result in a reduction in weight while maintaining impact performance, or increased impact performance for a given weight. The limitations of performing controlled impact experiments, especially at higher velocities, on composite and textile materials means that there is a need to study these events using numerical simulations.

Numerical investigations of ballistic fragment impacts on Polyethylene based fibre composite (Dyneema) [12] and Kevlar/Epoxy [13] body armour have been performed

at Century Dynamics and are briefly described below and compared with experimental work.

7.2.1 Ballistic Fragment Impacts on Aramid Composite Plates

An orthotropic material model coupled with a polynomial equation of state has been used to conduct numerical investigations of FSP (Fragment Simulating Projectile) impacts on Kevlar Fibre Reinforced Panel (KFRP) systems used for personal protective clothing armour [13]. Results of these investigations are shown below and compared with instrumented ballistic impact experiments carried out at TNO Prins Maurits Laboratory. The experiments included measurement of target back surface velocity during the impact using VISAR techniques.

In this work, the coupled anisotropic material model was used to simulate the case of a 1.1g steel fragment impacting an aramid composite plate at 483m/s. The Lagrange processor of AUTODYN-2D was used to represent both fragment and composite target.

The aramid composite comprised 19 layers of woven Kevlar 29 bonded in Epoxy. Basic quasi-static elastic properties for the composite were known although no dynamic material properties that would allow the derivation of non-linear shock terms were available. In the initial simulation work reported in [13], the material properties for Kevlar-129/Epoxy derived in [1] were used along with the polynomial equation of state. The 4340 steel fragment was represented using a Johnson-Cook strength model and data.

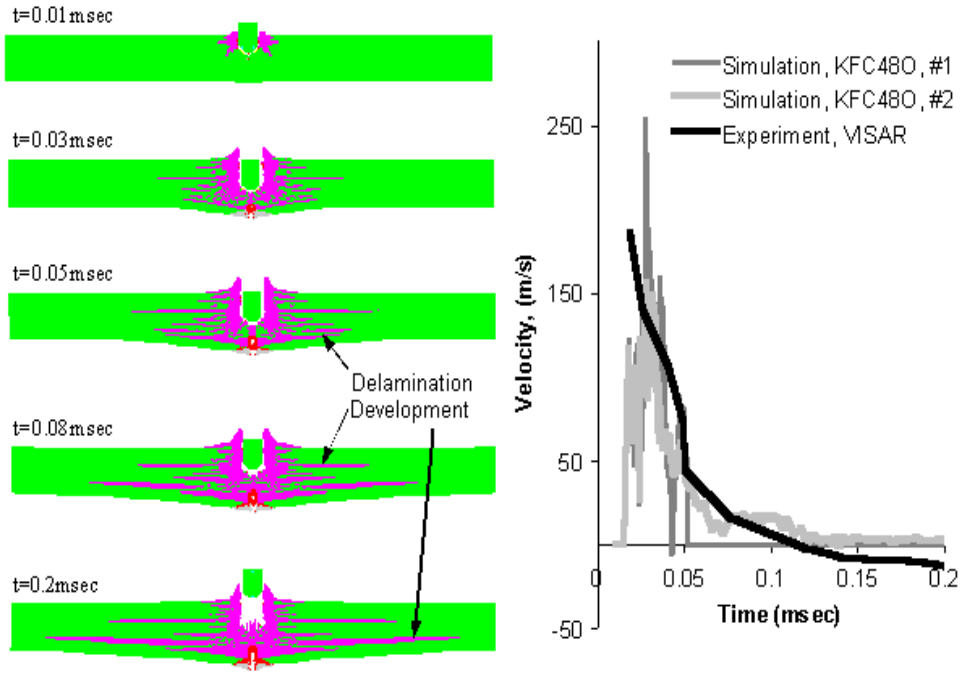

a) Simulated Damage Development **b) Back surface Velocity**

Figure 7-10 Fragment Impact on KFRP at 483m/s, Simulation and Experimental Results

7.2.2 Polyethylene fibre based armour

The performance of the orthotropic model coupled with a non-linear equation of state has been further evaluated for the ballistic performance of a new Dyneema (UD-

HB25) composite, which was being assessed by DCTA and TNO through an experimental testing programme [12]. Simulations of inverse flyer plate tests were conducted and a remarkable correspondence between test and simulation was obtained using the new composite model. The derived model was then successfully used to perform simulations of fragment impact tests and make an assessment of the V50 impact velocity. The model also reproduced, as illustrated in Figure 7-11, the deformation and delamination extent of the target plate.

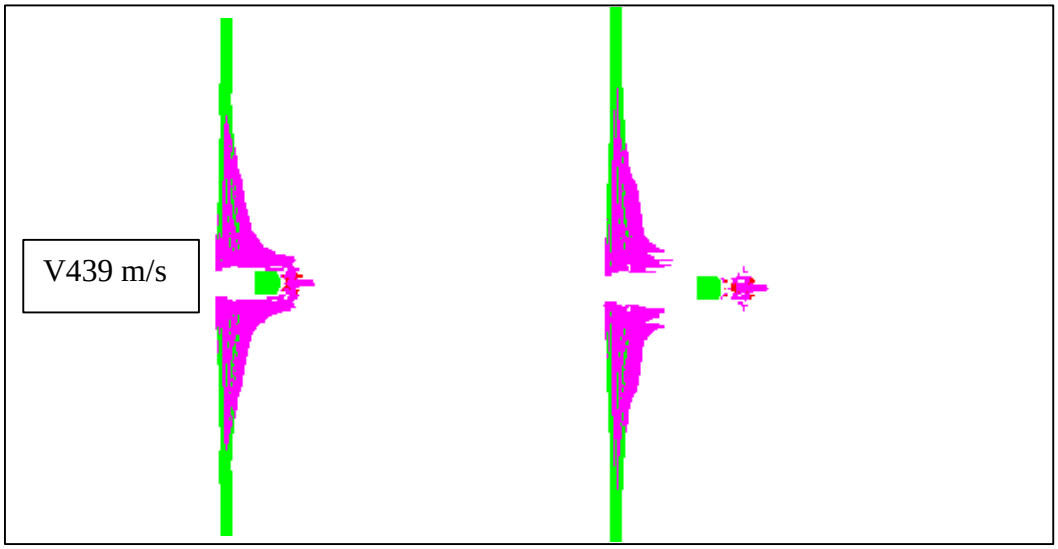

Figure 7-11 AUTODYN Simulations of 1.1g FSP Impacting 3.2mm Dyneema UDHB25 (Magenta Regions Indicate Delamination)

7.3 Bird Strike Example using Composite Shell Elements

A layered composite shell has been implemented in AUTODYN-3D. Composite shell elements allow efficient modelling of thin composite materials that are subjected to structural (rather than shock) type loading. All of the existing material models that are compatible with the standard shell element can be applied to individual layers of new composite shell elements. In addition the orthotropic equation of state can be used with the layered composite shell element. The composite shell always assumes that the 11 and 22 directions are in the plane of the shell and the 33 direction lies through the thickness.

An example composite shell application is shown in Figure 7-12 to Figure 7-14. Results from an AUTODYN simulation of a bird strike onto the leading edge of a composite tail plane are shown. Figure 7-12 and Figure 7-13 show the initial configuration of the bird and tail section. The bird has been modelled with SPH particles and the tail plane with a combination of composite and standard shell elements. The composite shells have been used to represent the layered GFRP and CFRP skin of the tail section. Figure 7-14 show material status plots for the tail section following the impact. Results for the outer and inner layers of the skin are shown.

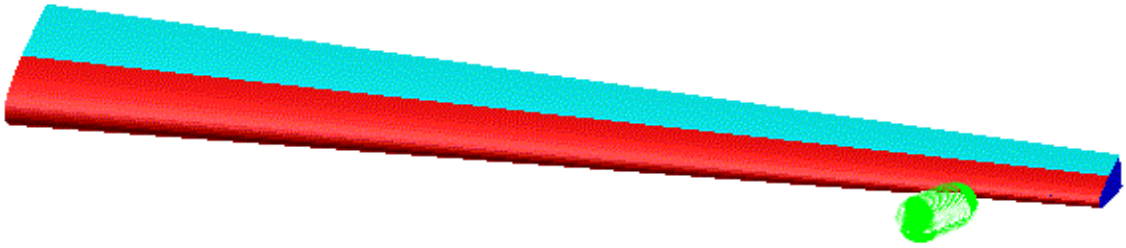

Figure 7-12 Initial configuration of composite tail section

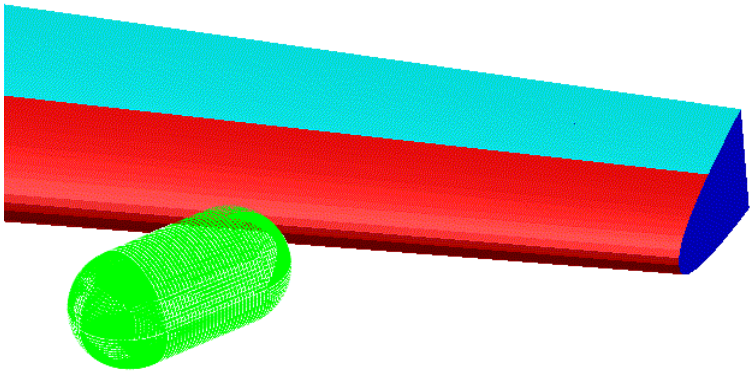

Figure 7-13 Initial configuration of composite tail section: Impact Zone

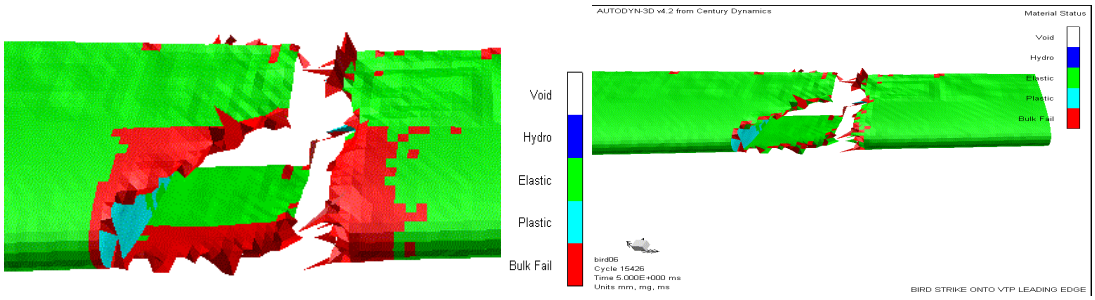

(a) Outer sublayer **(b) Inner sublayer**

Figure 7-14 Material Status following bird strike

8 Recommendations

AUTODYN contains many options for the modelling of composite materials. These options are described in detail in this report. However, in using these complex models the problems are often two fold; knowing which options/models to use and how/where to obtain the required material properties.

In 3 the various models are described in detail. It is important to take a pragmatic view of them rather than simply selecting the most complex. For example, if the application being modelled is only subjected to a relatively low speed impact then using an orthotropic material model with a linear equation of state is sufficient. In this case relatively simple experiments are required to obtain the directional strength properties or manufactures material data may be sufficient.

If the application is at ballistic velocities or higher then shock effects are most likely to be important and using a non-linear equation of state is recommended. However, this requires additional experiments as described in 5.2.1 in addition to the directional strength properties.

Whether or not the hardening option is required depends only upon the material being modelled. Some materials, such as carbon-epoxy composites have been observed to exhibit a very linear behaviour [14]. Other composite materials, like Kevlar-epoxy, are highly non-linear and significant hardening is observed [2]. In this case it is imperative to have the stress-strain data obtained from the experiments of 5.1 so that the plasticity parameters can be calculated as outlined in 6.1.2. Since the tension tests are usually performed to ultimate failure this experimental data will also indicate whether or not softening is significant.

9 References

[1] S. Hiermaier, W. Riedel, C.J. Hayhurst, R.A. Clegg, C.M. Wentzel, Advanced Material Models for Hypervelocity Impact Simulations, EMI-Report No. E43/99, ESA CR(P) 4305, 1999.

[2] W. Riedel, W. Harwick, D.M. White, R.A. Clegg, Advanced Material Damage Models for Numerical Simulation Codes, EMI-Report No. I 75/03, ESA CR(P) 4397, October 2003.

[3] J.K. Chen, F.A.Allahdadi, C.T.Sun, “A Quadratic Yield Function for Fiber-Reinforced Composites“, Journal of Composite Materials, vol. 31, No. 8, 1997.

[4] C.T. Sun and S. Li, “Three-Dimensional Effective Elastic Constants for Thick Laminates”, Journal of Composite Materials, vol. 22, 1988.

[5] C.E. Anderson, P.A. Cox, et. al. “A Constitutive Formulation for Anisotropic Materials Suitable for Wave Propagation Computer programme-II”, Comp. Mech., vol. 15, p201-223, 1994.

[6] J.P. Hou, N. Petrinic, C. Ruiz, “Prediction of Impact Damage in Composite Plates”, Comp. In Sc. and Tech., 60, 273-281, 2000.

[7] R.M. Jones, “Mechanics of Composite Materials”, McGraw-Hill, 1975.

[8] M.A. Meyers, “Dynamic Behaviour of Materials”, John Wiley & Sons, 1994 – ISBN 0-471-58262-X.

[9] W.C. Kim, C.K.H. Dharan, Analysis of five-point bending for determination of the interlaminar shear strength of unidirectional composite materials, Composite Structures, Vol. 30, 1995, 241-251.

[10] ASTM standard D3846-79 (1985), ASTM Standards and Literature References for Composite Materials, 2nd Ed., American Society for Testing and Materials, Philadelphia, PA, 1990.

[11] Luft- und Raumfahrt, Kohlenstoffaserverstärkte Kunstoffe, Prüfverfahren, Bestimmung der interlaminaren Energiefreisetzungsrate, Mode II,G/IIC, DIN EN 6034, April 1996.

[12] C.J. Hayhurst, J.G. Leahy, M. Deutekom, M. Jacobs, P. Kelly, “Development of Material Models for Numerical Simulation of Ballistic Impact onto Polyethylene Fibrous Armour”, presented at PASS, Colchester, UK, 2000.

[13] R.A. Clegg, C.J. Hayhurst, J.G. Leahy, M. Deutekom,. “Application of a Coupled Anisotropic Material Model to High Velocity Impact of Composite Textile Armour”, presented at the 18th Int. Symposium on Ballistics, San Antonio, USA, 1999

[14] D.M. White, E.A. Taylor, R.A. Clegg, “Numerical Simulation and Experimental Characterisation of Direct Hypervelocity Impact on a Spacecraft Hybrid Carbon Fibre/Kevlar Composite Structure”, Int. J. Impact Eng., vol. 29, 2003, pp779-790.